

A dipole anisotropy of galaxy distribution: Does the CMB rest-frame exist in the local universe?

Yousuke Itoh¹, Kazuhiro Yahata², Masahiro Takada³

¹ *Astronomical Institute, Graduate School of Science, Tohoku University, Sendai 980-8578, Japan*

² *Department of Physics, The University of Tokyo, Bunkyo-ku, Tokyo 113-0033, Japan*

³ *Institute of the Physics and Mathematics of the Universe (IPMU),
The University of Tokyo, Chiba 277-8582, Japan* *

The peculiar motion of the Earth causes a dipole anisotropy modulation in the distant galaxy distribution due to the aberration effect. However, the amplitude and angular direction of the effect is not necessarily the same as those of the cosmic microwave background (CMB) dipole anisotropy due to the growth of cosmic structures. In other words exploring the aberration effect may give us a clue to the horizon-scale physics perhaps related to the cosmic acceleration. In this paper we develop a method to explore the dipole angular modulation from the pixelized galaxy data on the sky properly taking into account the covariances due to the shot noise and the intrinsic galaxy clustering contamination as well as the partial sky coverage. We applied the method to the galaxy catalogs constructed from the Sloan Digital Sky Survey (SDSS) Data Release 6 data. After constructing the four galaxy catalogs that are different in the ranges of magnitudes and photometric redshifts to study possible systematics, we found that the most robust sample against systematics indicates no dipole anisotropy in the galaxy distribution. This finding is consistent with the expectation from the concordance Λ -dominated cold dark matter model. Finally we argue that an almost full-sky galaxy survey such as LSST may allow for a significant detection of the aberration effect of the CMB dipole having the precision of constraining the angular direction to ~ 20 degrees in radius. Assuming a hypothetical LSST galaxy survey, we find that this method can confirm or reject the result implied from a stacked analysis of the kinetic Sunyaev-Zel'dovich effect of X -ray luminous clusters in Kashlinsky et al. (2008,2009) if the implied cosmic bulk flow is not extended out to the horizon.

PACS numbers: 98.65.Dx

I. INTRODUCTION

The amplitude of the cosmic microwave background (CMB) dipole anisotropy is about two orders of magnitudes greater than the anisotropies at higher multipoles that are primarily generated during cosmic epochs until the last scattering surface of redshift $z \simeq 1100$. It is widely believed that the dipole anisotropy is produced by the Doppler effect due to the relative motion between the Earth, i.e. an observer, and the frame where the CMB looks nearly isotropic (hereafter we call it the CMB rest-frame). The measured CMB dipole amplitude tells that the relative velocity has an amplitude of $v_{\text{CMB}} \simeq 370 \text{ km s}^{-1}$ (1.23×10^{-3} in the unit $c = 1$) [1, 2]. The peculiar velocity consists of the five vector contributions [3]: the motion of the Earth around the solar system barycenter ($\sim 30 \text{ km s}^{-1}$), the motion of the solar system with respect to the Local Standard of Rest (LSR) [4], the (hypothetical circular) motion of the LSR around the Milky Way ($\sim 220 \text{ km s}^{-1}$ (the IAU 1985 recommended value), or $\sim 250 \text{ km s}^{-1}$ [5]), the motion of the Milky Way in the Local Group, and the motion of the Local Group with respect to the CMB rest-frame. The origin of the fifth component, the peculiar velocity of the Local Group, is still uncertain and has been under discussion over the past two decades (e.g., [6, 7] and also see [8, 9] and references therein). This peculiar velocity is believed to be generated by the spatial inhomogeneities of mass (mainly dark matter) distribution in nearby large scale structures via gravitational instability as predicted in the cold dark matter (CDM) dominated structure formation scenario. Therefore the peculiar velocity field is expected to reflect properties of structure formation in the low-redshift Universe. For example, the peculiar velocity of the Local Group with respect to the CMB rest-frame is estimated to be $\sim 600 \text{ km s}^{-1}$, based on the result of [3]. This is greater than the rms amplitude of the peculiar velocity, $\sim 470 \text{ km s}^{-1}$, predicted from the linear theory of the concordance Λ CDM model. However, due to the difficulties in inferring the mass distribution from the observed galaxy distribution, i.e. the galaxy bias uncertainty, the origin of the peculiar velocity is not yet fully understood [10–14].

*Electronic address: yousuke@astr.tohoku.ac.jp

Then a naive question may arise; how special is the CMB rest-frame? One may think that cosmic large-scale structures have formed via gravitational instability over 13.7G years in the CMB rest-frame. In other words, the Universe may still stay in the CMB rest-frame over the cosmic age [59]. However, a possibility has been discussed that the CMB rest-frame may not coincide with the rest frame of galaxy distribution due to super-horizon scale physics [15, 16]. In fact, the present-day Universe is in the mysterious phase, the cosmic accelerating phase. The origin of the cosmic acceleration is one of the most profound problems in modern cosmology and physics, and it is sometimes discussed that the cosmic acceleration is perhaps related to the horizon-scale physics. For example, while dark energy is one possible explanation of the cosmic acceleration, dark energy should have spatial perturbations inevitably on horizon scales, if it is not a cosmological constant (e.g. [17, 18] and references therein). Or the primordial power spectrum, produced in the inflationary era, may have weird behaviors on horizon scales such as the truncated power spectrum as speculated from the low CMB quadrupole amplitudes (e.g., [19–21]). Thus exploring the rest frame of the present-day Universe may give a clue to the horizon-scale physics (also see [16]). Furthermore, this may give an independent test on the cosmological principle, the isotropy and homogeneity of the Universe.

The rest frame of the present-day Universe may be defined by the frame where the galaxy distribution looks isotropic on a sufficiently large scale (hereafter we will call it the matter rest-frame or the rest-frame of the local Universe). The relative motion of the Earth to the matter rest-frame causes a dipole anisotropy modulation in the observed galaxy distribution [15]. The dipole anisotropy is caused by the two effects. First, photons from galaxies ahead of/behind the Earth are blue-/red-shifted by the Doppler effect, causing their fluxes to be brightened/dimmed and therefore the galaxies to be included/excluded in the magnitude limited sample. Secondly, special relativity predicts the aberration of angles causing the surface number density of galaxies to be enhanced/suppressed in the direction ahead of/behind us, even if the intrinsic galaxy distribution is perfectly homogeneous on the sky. If the motion has a similar amplitude inferred from the CMB dipole, the induced dipole modulation is small at a sub-percent level. Hence a large-area survey of distant galaxies or radio sources is suited for exploring this dipole anisotropy, because the intrinsic galaxy clustering that has greater amplitudes at low redshifts may cause a significant contamination. There have been many attempts made to explore this dipole anisotropy from such surveys [22–24]. In particular Blake and Wall [24] analyzed the radio source distribution based on the NRAO VLA Sky Survey (NVSS) data [25], and then claimed a possible detection of the dipole anisotropy that are consistent with the CMB dipole in the amplitude and direction within 2σ and 1σ levels, respectively.

The purpose of this paper is to explore the cosmological dipole signature from the galaxy catalogs constructed from the Sloan Digital Sky Survey (SDSS) Data Release 6 (DR6) data [26]. The use of the photometric SDSS galaxy sample has several advantages: the sky coverage is large (about 20% of the full sky), the photometry is well-calibrated and the photometric redshift information of each galaxy is available. In doing this, we develop a method to explore the dipole modulation in a pixelized galaxy distribution properly taking into account the covariances due to the Poisson shot noise and the intrinsic clustering contamination as well as the partial sky coverage. In particular the photometric redshift information of SDSS galaxies is useful to reduce the clustering contamination from nearby structures. Furthermore, we will discuss how a planned large-area galaxy survey such as the Large Synoptic Survey Telescope (LSST) can be useful to explore the dipole anisotropy.

Here it may be worth mentioning advantages and shortcomings of our method compared to the peculiar velocity field studies [9–14]. This paper concerns with the dipole pattern in the galaxy distribution due to the observer’s motion with respect to the matter rest-frame. Comparing this and CMB dipole anisotropies can address if the inferred matter rest-frame agrees with the CMB rest-frame within the measurement errors. This paper does not discuss the origin of our motion (or the motion of the Local Group) nor which structures in the Local Group cause our motion with respect to the CMB rest-frame, the so-called convergence depth. This question is one of the main questions discussed in the recent peculiar velocity field studies [9–14].

The structure of this paper is as follows. After reviewing the aberration effect on the galaxy counts of a given magnitude limit in Sec. II, we will develop a method to explore the induced dipole modulation from a galaxy catalog properly taking into account the covariance and the partial sky coverage in Sec. III. In Sec. IV, we make an estimate on the detectability of the aberration effect from the galaxy distribution for hypothetical galaxy surveys, SDSS- and LSST-type surveys, *assuming* that the Earth’s relative motion to the matter rest-frame has the same amplitude with the CMB dipole. Sec. V shows the main results of this paper. After defining the galaxy catalogs based on the magnitude range and the photometric redshift information and then estimating the covariance matrix of the pixelized galaxy counts on the sky, we will show the results for an exploration of the dipole anisotropy from the SDSS DR6 galaxy catalogs where the amplitude and angular direction of the aberration effect are treated as free parameters. In Sec. VI we will also discuss the forecast for an LSST-type survey. Sec. VII is devoted to summary and discussion. Throughout this paper we will employ the concordance Λ CDM model that is specified by $(h, \Omega_\Lambda, \Omega_m h^2, \Omega_b h^2, \sigma_8, n_s) = (0.73, 0.762, 0.127, 0.0223, 0.74, 0.951)$ [27].

II. EFFECT OF THE EARTH'S PECULIAR MOTION ON THE ANGULAR NUMBER DENSITY FIELDS OF GALAXIES

Even if there exists the *matter rest-frame* where the intrinsic galaxy distribution looks perfectly isotropic, the peculiar motion of the Earth relative to the matter rest-frame induces an apparent angular modulation in the galaxy number density field on the sky [15]. There are two effects that cause this modulation. The first is the aberration effect, causing the observed number density field to be increased or decreased in the angular direction forward or backward of the Earth's motion, respectively. The second is the Doppler effect: depending on the shape of spectral energy density of a galaxy, the Doppler effect causes the apparent magnitude of galaxy to be brighter or fainter, leading the galaxy to be included into or excluded from the magnitude limited sample. The net effect arises from the linear sum of these two effects in a case that the peculiar velocity is much smaller than the speed of light.

In the following, we will in more detail model the effect of the Earth's peculiar motion on the angular number counts of galaxies defined for a given limiting magnitude. In so doing, we assume for clarity that the galaxy distribution is perfectly isotropic on the sky in the matter rest-frame, and in other words we ignore intrinsic anisotropies in the galaxy distribution arising from large-scale structure formation. We shall come back to the intrinsic anisotropy contamination later.

Special Relativity predicts that, due to aberration of angle, the relative velocity of an observer to the matter rest-frame causes the angular position of a galaxy observed on the sky to be displaced:

$$\tan \phi_{\text{obs}} = \frac{\sqrt{1 - \beta^2} \sin \phi}{\cos \phi + \beta} \approx \frac{\sin \phi}{\cos \phi + \beta}, \quad (1)$$

where ϕ_{obs} denotes the angle between the direction of the galaxy seen by the observer and the direction of the observer's velocity \mathbf{v} , ϕ is the corresponding angle in the matter rest-frame, and $\beta \equiv |\mathbf{v}|/c$. In the second equality on the r.h.s. we assumed $\beta \ll 1$, and ignored the term of $O(\beta^2)$. In the following we will similarly ignore the contribution of $O(\beta^2)$ for simplicity. The conservation of the number of galaxies tells that the observer sees an angular modulation in the galaxy distribution as a function of the angular direction $\boldsymbol{\theta}$ on the celestial sphere:

$$n(\boldsymbol{\theta}) = \frac{d\phi}{d\phi_{\text{obs}}} \approx \bar{n} (1 + 2\beta \cos \alpha), \quad (2)$$

where $\boldsymbol{\theta} = (\cos \theta \cos \varphi, \cos \theta \sin \varphi, \sin \theta)$ for the spherical coordinates (we have employed the continuous field limit, which is a good approximation for cases of interest) and \bar{n} is the intrinsic number counts per unit steradian. The angle α is defined by $\cos \alpha \equiv \boldsymbol{\theta} \cdot \hat{\mathbf{v}}$, where $\hat{\mathbf{v}}$ denotes the angular direction of the Earth's peculiar velocity \mathbf{v} on the celestial sphere and is fully specified by two parameters.

Next let us consider the Doppler effect on the galaxy counting. Besides redshift due to the cosmic expansion, the peculiar velocity of an observer relative to the comoving rest frame of galaxy distribution causes a photon emitted from a galaxy to be redshifted or blueshifted depending on the angular direction of the galaxy relative to the peculiar velocity direction. The observed frequency ν_{obs} is related to the rest frame frequency ν_{rest} via

$$\eta \equiv \frac{\nu_{\text{obs}}}{\nu_{\text{rest}}} = \frac{1 + \beta \cos \phi}{(1 - \beta^2)^{1/2}} \approx 1 + \beta \cos \phi, \quad (3)$$

where the angle ϕ is defined in the same way as in Eq. (1). If we assume that an intrinsic flux density of a galaxy [in the units of $\text{erg s}^{-1} \text{cm}^{-2} \text{Hz}^{-1}$] is simply given by a power law as $S_{\text{rest}}(\nu) \propto \nu^p$, the conservation of photon number tells that the observed flux density $S_{\text{obs}}(\nu)$ is expressed as

$$S_{\text{obs}}(\nu_{\text{obs}}) = S_{\text{rest}}(\nu_{\text{rest}}) \frac{\nu_{\text{obs}}}{\nu_{\text{rest}}} \frac{d\nu_{\text{rest}}}{d\nu_{\text{obs}}} \frac{dt_{\text{rest}}}{dt_{\text{obs}}} = \eta^{1-p} S_{\text{rest}}(\nu_{\text{obs}}). \quad (4)$$

The apparent magnitude of the galaxy in a given filter is obtained by integrating the flux density over a range of transmission frequencies of the filter, and therefore the observed magnitude, m_{obs} , is related to the rest frame magnitude, m_{rest} , via

$$m_{\text{obs}} = m_{\text{rest}} - 2.5(1 - p) \log_{10} \eta. \quad (5)$$

If we assume that the intrinsic number counts of galaxies, where galaxies brighter than a given limiting magnitude m_{lim} are included in the sample, is simply given by

$$\bar{n}(m < m_{\text{lim}}) \propto 10^{xm_{\text{lim}}}, \quad (6)$$

with x being a numerical coefficient of order unity [28], the observed number counts are found from Eqs. (3) and (5) to be

$$\begin{aligned} n(\boldsymbol{\theta}; m < m_{\text{lim}}) &= \bar{n}(m < m_{\text{rest,lim}} = m_{\text{lim}} + 2.5(1-p) \log_{10} \eta) \\ &= \eta^{2.5x(1-p)} \bar{n}(m < m_{\text{lim}}) \\ &\approx [1 + 2.5x(1-p)\beta \cos \alpha] \bar{n}(m < m_{\text{lim}}), \end{aligned} \quad (7)$$

where the angle α is defined in the same way as in Eq. (2).

Hence, taking into account both the aberration effect (2) and the Doppler effect (7) up to the first order of β , the observed angular number density field of galaxies for the limiting magnitude m_{lim} is expressed as

$$n(\boldsymbol{\theta}; m < m_{\text{lim}}) = \bar{n}(m < m_{\text{lim}}) \left[1 + 2\tilde{\beta} \cos \alpha \right], \quad (8)$$

with the modified β parameter defined as [60]

$$\tilde{\beta} = [1 + 1.25x(1-p)] \beta. \quad (9)$$

Note again that the dependence of $n(\boldsymbol{\theta})$ on angular direction $\boldsymbol{\theta}$ comes through the relation $\cos \alpha \equiv \boldsymbol{\theta} \cdot \hat{\mathbf{v}}$. Eq. (8) shows that the Earth's motion relative to the matter rest-frame induces a characteristic dipole pattern in the angular number density field of galaxies. The dipole pattern is fully specified by 3 parameters: $\tilde{\beta}$ and 2 parameters for $\hat{\mathbf{v}}$. The average of Eq. (8) over the whole sky indeed satisfies conservation of the total number of galaxies:

$$\frac{1}{4\pi} \oint_{4\pi} d\Omega_{\boldsymbol{\theta}} n(\boldsymbol{\theta}) = \bar{n}. \quad (10)$$

If the matter rest-frame is the same as the CMB rest-frame with respect to which the Earth is moving with the velocity $\beta \approx (1.231 \pm 0.008) \times 10^{-3}$ in the direction $(l, b) = (264^{\circ}31 \pm 0^{\circ}04 \pm 0^{\circ}16, 48^{\circ}05 \pm 0^{\circ}02 \pm 0^{\circ}09)$ in the Galactic coordinates [1, 2], the dipole amplitude is $O(\beta) \sim O(10^{-3})$ as the prefactor in Eq. (9) in front of β is of the order of unity for the number counts of galaxies in optical passbands [28–30]. To detect the dipole pattern in the galaxy distribution, a galaxy survey with full sky coverage is ideally needed, while a partial-sky survey such as SDSS makes it less straightforward to explore the dipole pattern, because the galaxy distribution displays a smaller angular modulation over the sky region observed, as will be discussed below.

III. METHODOLOGY: A χ^2 TEST FOR DETECTING THE ABERRATION EFFECT

In reality, a galaxy distribution actually seen is quite far from homogeneous, rather displaying rich, hierarchical structures on various distance scales – cosmic large-scale structures. To measure the aberration effect due to the Earth's peculiar velocity, we need to discriminate the effect from the inhomogeneities due to large-scale structures. In addition we have to take into account observational effects such as the survey geometry and the shot noise contamination due to a finite number of galaxies. In this section we develop a methodology for measuring the aberration effect from a wide-field galaxy survey, which will be applied to the SDSS data in subsequent sections.

For an actual galaxy survey, the density perturbation field has to be estimated from the discrete distribution of galaxies. Since the dipole modulation of interest appears over an angular scale of π radian and we are not interested in small angular scales, it is convenient to consider a pixelized map of galaxy distribution, where the pixel size greater than degree scales would be sufficient for our purpose. We define the number density of galaxies in the i -th pixel as

$$n_{\text{obs}}(\boldsymbol{\theta}_i) = \sum_{j=1}^{N_{\text{gal,tot}}} \int_{\Omega_S} d^2\Omega_{\boldsymbol{\theta}} W_{(i)}(\boldsymbol{\theta}_i - \boldsymbol{\theta}) \delta_D^2(\boldsymbol{\theta} - \boldsymbol{\theta}_{g,j}), \quad (11)$$

where $\boldsymbol{\theta}_i$ denotes the angular position of the i -th pixel, given by $\boldsymbol{\theta}_i = (\sin \theta_i \cos \varphi_i, \sin \theta_i \sin \varphi_i, \cos \theta_i)$ in the celestial polar coordinates, $\delta_D^2(\boldsymbol{\theta})$ is the Delta function, $\boldsymbol{\theta}_{g,j}$ denotes an angular position of the j -th galaxy, and the summation \sum_j runs over all the galaxies used in the analysis, $j = 1, 2, \dots, N_{\text{gal,tot}}$ ($N_{\text{gal,tot}}$ is the total number). Note that the integration $\int_{\Omega_S} d^2\Omega_{\boldsymbol{\theta}}$ is confined to the survey region with area Ω_S . The window function $W_{(i)}(\boldsymbol{\theta})$ defines the pixel shape normalized as $\int d^2\boldsymbol{\theta} W_{(i)}(\boldsymbol{\theta}) = 1$, where the subscript (i) is used for notational convenience to explicitly imply that the window function may change by pixel-to-pixel taking into account possible variations due to the pixel geometry, masking and so on. For example, a top-hat type window function is given by $W_{(i)}(\boldsymbol{\theta}) = 1/(\pi\theta_{\text{pix}(i)}^2)$ if $|\boldsymbol{\theta}| < \theta_{\text{pix}(i)}$, otherwise zero.

For our purpose we need to deal with the density perturbation field defined as

$$\delta_{\text{obs}}(\boldsymbol{\theta}_i) = \frac{n_{\text{obs}}(\boldsymbol{\theta}_i)}{N_{\text{gal,tot}}/\Omega_S} - 1, \quad (12)$$

Note that the $N_{\text{gal,tot}}/\Omega_S$ is an estimate on the average number density for a given survey.

Accordingly we need to modify a modeling of the aberration effect such that the model prediction can be compared with the pixelized galaxy distribution above: the number density in the i -th pixel can be simply modeled from Eq. (8) as

$$n_{\text{model}}(\boldsymbol{\theta}_i) = \bar{n} \left[1 + 2\tilde{\beta} \cos \alpha_i \right], \quad (13)$$

where $\cos \alpha_i \equiv \boldsymbol{\theta}_i \cdot \hat{\mathbf{v}}$. However, when a survey has a partial sky coverage, the conservation law (10) no longer holds. In other words,

$$\int_{\Omega_S} \frac{d\Omega_{\boldsymbol{\theta}}}{\Omega_S} n(\boldsymbol{\theta}) = \bar{n} \left(1 + 2\tilde{\beta} \int_{\Omega_S} \frac{d\Omega_{\boldsymbol{\theta}}}{\Omega_S} \cos \hat{\mathbf{v}} \cdot \boldsymbol{\theta} \right) \neq \bar{n}, \quad (14)$$

where Ω_S is the survey area, and the integration range is confined to the survey region. Hence, the average number density \bar{n} in Eq. (13) needs to be estimated taking into account the partial sky coverage: the model density perturbation field, just like the derivation in Eq. (12), is modified as

$$\begin{aligned} \delta_{\text{model}}(\boldsymbol{\theta}_i) &\equiv \frac{1 + 2\tilde{\beta} \cos \alpha_i}{(1/\Omega_S) \sum_{j=1}^{N_{\text{pix}}} \Omega_{\text{pix}(j)} (1 + 2\tilde{\beta} \cos \alpha_j)} - 1 \\ &\simeq 2\tilde{\beta} \left[\cos \alpha_i - \frac{1}{\Omega_S} \sum_{j=1}^{N_{\text{pix}}} \Omega_{\text{pix}(j)} \cos \alpha_j \right], \end{aligned} \quad (15)$$

where the summation runs over all the pixels used (N_{pix} is the total number). Note that the denominator in the first line gives an estimate on the average number density for a case of the partial sky coverage, and the averaging of the aberration effect is weighted by the pixel area, $\Omega_{\text{pix}(j)}$.

In this paper, to measure the aberration effect for a given galaxy survey, we employ a simplest statistic χ^2 . From Eqs. (12) and (15), the χ^2 statistic can be given by

$$\chi^2(\hat{\mathbf{v}}, \tilde{\beta}) \equiv \sum_{i,j=1}^{N_{\text{pix}}} \left[\delta_{\text{obs}}(\boldsymbol{\theta}_i) - \delta_{\text{model}}(\boldsymbol{\theta}_i; \hat{\mathbf{v}}, \tilde{\beta}) \right] [\mathbf{C}]_{ij}^{-1} \left[\delta_{\text{obs}}(\boldsymbol{\theta}_j) - \delta_{\text{model}}(\boldsymbol{\theta}_j; \hat{\mathbf{v}}, \tilde{\beta}) \right], \quad (16)$$

where $[\mathbf{C}]^{-1}$ is the inverse of the covariance matrix as explained below. The best-fit model parameters for $\hat{\mathbf{v}}$ and $\tilde{\beta}$, 3 parameters in total, can be estimated by minimizing the χ^2 value with varying the model parameters freely, given the pixelized galaxy distribution.

The statistical uncertainty in measuring the aberration effect is quantified by the covariance matrix \mathbf{C} in Eq. (16). Following [31] (see Sec. 31; also see [32]), the covariance matrix \mathbf{C}_{ij} is found to be given by

$$\mathbf{C}_{ij} = \frac{\delta_{ij}^K}{N_{g(i)}} + w_g(\theta_{ij}), \quad (17)$$

where $\theta_{ij} \equiv \cos^{-1}(\boldsymbol{\theta}_i \cdot \boldsymbol{\theta}_j)$, δ_{ij}^K is the Kronecker delta function, $N_{g(i)}$ is the number of galaxies contained in the i -th pixel, and $w_g(\theta)$ is the angular two-point correlation function of the pixelized galaxy distribution. The first term gives the shot noise contamination due to a finite number of galaxies, while the second term quantifies the sampling variance originating from the intrinsic galaxy clustering in large-scale structure. Note that the second term is non-vanishing when $i \neq j$, which describes how the errors between different pixels are correlated with each other. The covariance matrix \mathbf{C} has a dimension of $N_{\text{pix}} \times N_{\text{pix}}$.

The two-point correlation function $w_g(\theta)$ in Eq. (17) can be expressed in terms of the angular power spectrum of galaxy distribution, $C_g(l)$, as

$$w_g(\theta_{ij}) = \sum_{l=1}^{\infty} \frac{2l+1}{4\pi} C_g(l) \tilde{W}_{(i)}(l\Theta_{\text{pix}(i)}) \tilde{W}_{(j)}^*(l\Theta_{\text{pix}(j)}) P_l(\cos \theta_{ij}), \quad (18)$$

Survey	Area (Ω_S) (deg ²)	$N_{\text{gal,tot}}/\Omega_S$ (deg ⁻²)	z_m	A_{ab}	A_{LSS}	A_P	S/N
SDSS-like ($f_{\text{sky}} \approx 0.19$)	7838	487	~ 0.3	5.3×10^{-4}	1.3×10^{-3}	2.8×10^{-4}	0.40
low- z full-sky ($f_{\text{sky}} = 1$)	41200	487	~ 0.3	2.4×10^{-3}	2.8×10^{-3}	6.6×10^{-4}	0.84
LSST-like ($f_{\text{sky}} \simeq 0.46$)	19000	9.7×10^4	1.2	1.2×10^{-3}	2.1×10^{-4}	3.2×10^{-5}	5.5

TABLE I: A rough estimates of the expected signal to noise ratios for three survey configurations. The ‘‘SDSS-like’’ survey assumes the survey geometry, galaxy redshift distribution and galaxy number density of the SDSS DR6 for survey parameters. The ‘‘low- z full-sky’’ survey assumes the full sky coverage, but other parameters are the same as the SDSS parameters. The ‘‘LSST-like’’ survey assumes the configuration of the future LSST which will be explained in Sec. VI. The notations are as follows. $f_{\text{sky}} = \Omega_S/(4\pi)$: the sky coverage of the survey. $N_{\text{gal,tot}}/\Omega_S$: the average number density of galaxies per unit square degrees. z_m : the mean redshift of the galaxy distribution. A_{ab} : the dipole amplitude coefficient of the aberration effect assuming the CMB dipole amplitude, $\tilde{\beta} = \beta \approx 1.231 \times 10^{-3}$, where the survey geometry is also taken into account. A_{LSS} : the dipole amplitude coefficient expected from angular galaxy clustering in large-scale structures. A_P : the dipole amplitude coefficient expected from the Poisson noise due to a finite number density of galaxies. S/N : the estimated signal-to-noise (S/N) ratio for measuring the aberration effect.

where $\tilde{W}_{(i)}(x)$ is the Fourier transform of the i -th pixel’s window function $W_{(i)}(x)$, and $P_l(x)$ is the l -th order Legendre polynomial function. The symbol $*$ denotes the complex conjugate. Assuming a linear bias model between the matter and galaxy distributions, which is a good approximation on angular scales of interest, the angular power spectrum $C_g(l)$ can be expressed in terms of the underlying linear power spectrum of mass perturbations as

$$C_g(l) = \frac{2}{\pi} b_g^2 \int_0^\infty P_m^L(k) |I_l(k)|^2 k^2 dk, \quad (19)$$

with

$$I_l(k) = \int_0^\infty D(z) n_g(z) j_l(kr(z)) dz, \quad (20)$$

where b_g is the linear bias parameter of galaxies, r is the comoving angular-diameter distance, $D(z)$ is the linear growth rate normalized as $D(z=0) = 1$ today, $n_g(z)$ is the redshift distribution of galaxies normalized as $\int_0^\infty n(z) dz = 1$, $j_l(x)$ is the l -th order spherical Bessel function, and $P_m^L(k)$ is the linear mass power spectrum today. The CDM based linear perturbation theory provides secure predictions for $P_m^L(k)$ as a function of cosmological parameters [e.g., see 33]. Once the CDM model and the galaxy bias are assumed and the galaxy redshift distribution is estimated or known, one can make a secure estimate of the sample variance contribution to the covariance. We will use the FFTLog code developed in [34] to compute the z -integration in Eq. (20) (also see [35]). An alternative method is to use the angular correlation function measured from the survey itself, however, it is generally difficult to obtain an accurate measurement of $w_g(\theta)$ on large angular scales we are interested in.

IV. A ROUGH ESTIMATE ON THE SIGNAL-TO-NOISE FOR A GALAXY SURVEY

Before going to the results, it would be useful to have a rough estimate on the signal-to-noise ratio for measuring the aberration effect from a given galaxy survey. As discussed in Sec. III, the measurement is contaminated by the shot noise of discrete galaxy distribution and the galaxy clustering contribution in large-scale structures. Here we simply compare the expected dipole amplitude due to the aberration effect with those of the contaminating effects, taking into account the survey geometry (see [36] for the details). A detailed derivation of the equations used in this section is also given in the appendix A.

As partially discussed in Sec. III, an incomplete sky coverage dilutes the dipole modulation in the galaxy distribution. For the case of a partial survey coverage, the dipole amplitude of the aberration effect is estimated as

$$A_{\text{ab}} \equiv 2\tilde{\beta} \sqrt{\frac{S_{11}}{3}}. \quad (21)$$

The quantity S_{11} takes into account the dilution effect due to the survey geometry and is found to be given by

$$S_{ll'} \equiv \sum_{m=-l}^l \sum_{m'=-l'}^{l'} |W_{ll'}^{mm'}|^2, \quad (22)$$

with the window function $W_{l'}^{mm'}$ being defined in [37] as

$$W_{l'}^{mm'} \equiv \oint d\Omega_{\boldsymbol{\theta}} Y_l^m(\boldsymbol{\theta}) Y_{l'}^{m'*}(\boldsymbol{\theta}) M(\boldsymbol{\theta}), \quad (23)$$

where Y_l^m is the spherical harmonic function and $M(\boldsymbol{\theta})$ is the mask function to define the survey region: $M(\boldsymbol{\theta}) = 1$ if the angular position $\boldsymbol{\theta}$ is inside the survey region, otherwise zero.

The dipole component arising from the clustering distribution of galaxies can be characterized by the angular power spectrum, weighted with the survey window function. Following the method developed in [36], the dipole amplitude can be estimated as

$$A_{\text{LSS}} = \sqrt{\frac{3}{4\pi}} \sqrt{\sum_{l'=1}^{\infty} S_{1l'} C_g(l')}, \quad (24)$$

where the prefactor $\sqrt{3/4\pi}$ is from the definition of the first-order spherical harmonic function, $Y_1^0 = \sqrt{3/4\pi} \cos \theta$. The partial sky coverage causes the power spectra of all the l' -th orders, $C_g(l')$, to contribute to the dipole amplitude.

The dipole amplitude arising from the shot noise due to the discrete galaxy distribution is similarly estimated as

$$A_P = \frac{3}{\sqrt{4\pi}} \sqrt{\frac{\Omega_S}{4\pi \bar{n}_g}}. \quad (25)$$

Note that $1/\bar{n}_g$ is the inverse of the average angular number density of galaxies per steradian.

Hence, from Eqs.(21), (24) and (25), the signal-to-noise ratio for measuring the aberration effect may be estimated as

$$\frac{S}{N} = \frac{A_{\text{ab}}}{\sqrt{A_{\text{LSS}}^2 + A_P^2}}. \quad (26)$$

The S/N simply assesses the dipole amplitude of the aberration effect relative to those of the contaminating effects.

Table I gives the estimates on S/N for three types of galaxy surveys assuming the CMB dipole amplitude for the aberration effect, assuming $\tilde{\beta} = \beta = 1.231 \times 10^{-3}$. First we consider a ‘SDSS-like survey’ that mimics the SDSS galaxy distribution analyzed in this paper, including the survey geometry, the total number of galaxies and the redshift distribution. In this case $S/N \simeq 0.4$, smaller than unity, meaning that the aberration effect is difficult to measure. Comparing the dipole amplitudes, A_{ab} , A_{LSS} , and A_P clarifies that A_{LSS} gives a significant contamination to an extraction of the aberration effect. To study the impact of the partial sky coverage, the row labeled as ‘full-sky’ shows the results when considering the full-sky coverage but keeping other survey parameters to be the same as those for the SDSS-like survey. The aberration signal becomes more significant, however, the clustering dipole amplitude contamination is still significant, resulting only in a slight improvement as $S/N \simeq 0.8$. On the other hand, the LSST-like survey that probes the galaxy distribution up to much higher redshifts and with a wide sky coverage $f_{\text{sky}} \approx 0.46$ is found to allow for a significant detection of the aberration effect, $S/N \simeq 5.5$, more than 5σ . Therefore these results show that it is more important to probe the galaxy distribution at *higher* redshifts for measuring the aberration effect mainly because of the following two reasons. First, the galaxy distribution is less evolving and more in the linear regime at higher redshifts, therefore the clustering dipole less contaminates to the dipole signal. Second, while the cosmic structures at smaller distance scales are more rapidly evolving towards the nonlinear regime in the CDM structure formation scenario, the small-scale structures at *higher* redshifts are viewed by an observer with smaller angles, less contributing to the dipole amplitude appearing at large angular scales.

V. APPLICATION TO SDSS DR6 PHOTOMETRIC GALAXIES SAMPLE

The SDSS 6th Data Release (DR6) [26, 38] covers about 8000 deg^2 of sky area and contains over 200 million of objects with photometry in five pass bands: u, g, r, i , and z [39, 40]. The SDSS galaxy sample would be a most suitable data set to explore the aberration effect because of the well-calibrated, homogeneous photometric and astrometric properties.

A. Constructing Galaxy Samples from the SDSS Photometric Galaxy Catalog

We construct the galaxy sample from the SDSS photometric catalog following [41]. There are several uncertainties in the photometric calibration that may cause artificial angular modulations in the galaxy distribution, such as an

imperfect correction of Galactic dust extinction and the contamination of stars to the sample caused by an imperfect start-galaxy separation. We will also use photometric redshift (hereafter, simply photo- z) information of each galaxy to define our galaxy sample. We will below briefly describe the definition of our galaxy sample.

1. Dust extinction correction

An inaccurate correction of Galactic dust extinction may cause artificial angular modulations in the galaxy distribution that is defined for a magnitude-limited sample. In the SDSS database, each object has information on not only its photometric properties but also the dust extinction estimated based on the Galactic dust extinction map in [42] (hereafter SFD), $A_{x,SFD}$, ($x = u, g, r, i$, and z). As carefully investigated in [41], there may remain a small systematic bias in the extinction correction, especially in the field with $A_{r,SFD} < 0.1$. However, the possible systematics has not been yet resolved, so we adopt the magnitudes where dust extinction was corrected for based on the SFD map.

2. Star-galaxy separation

A secure galaxy-star separation is also important, because star contamination to the galaxy sample likely causes angular modulations in the galaxy number counts towards the Galactic plane. We constructed a photometric galaxy sample taking the following three steps:

1. False objects were discarded using photometric processing flags. Namely, we removed the photometric objects that have saturated fluxes, were observed during bad sky conditions or are identified as fast-moving objects.
2. Masked regions were excluded, where the masked regions are defined from regions labeled as “BLEEDING”, “BRIGHT STAR”, “TRAIL”, or “HOLE”.
3. The magnitude range to define the galaxy sample was employed to ensure a reliable star-galaxy separation.

The details on Step 1 and 2 can be found in [41]. In Step 3 we employed the two i -band magnitude ranges: $19.1 \leq m_i \leq 19.6$ and $19.6 \leq m_i \leq 20.1$, respectively.

3. Reducing a clustering dipole

Nearby non-linear structures are viewed by an observer on relatively larger angular scales after projection. This causes a contamination to our seeking of the aberration effect because the galaxy clustering on small scales contaminates to the dipole amplitude for a survey with partial sky coverage. For example, the apparent galaxy distribution in the nearby large scale structures, which extends up to $\sim 60 - 200 \text{ Mpc}h^{-1}$ in radial distance, is away from the CMB dipole direction only by $\sim 10 - 20$ degrees on the sky [e.g. 10–12]. In addition, from the SDSS galaxy catalog itself, the apparent galaxy concentration at $z \sim 0.08$, the so-called “Sloan Great Wall”, has been found [43], and is away from the CMB dipole direction only by ~ 10 degrees. Thus including such nearby non-linear structures in the galaxy sample may apparently enhance large-angle clustering amplitudes in the galaxy distribution toward the local structures, which in turn prevents us from detecting the aberration effect due to the Earth’s peculiar motion relative to the rest-frame of the SDSS galaxy distribution at typical redshifts $z \sim 0.3$. Hence, to maximize a chance to detect the aberration effect on the SDSS galaxy sample, it is desirable to remove such nonlinear structures at low redshifts as much as possible.

For the reasons mentioned above, we use photometric redshift information to define a secure galaxy sample. Fig. 1 shows the photometric redshift distribution of SDSS galaxies per unit steradian as a function of i -band magnitudes. One can see that the SDSS photometric galaxy sample has a typical redshift of $z \sim 0.3$. However, there also appears too large population of galaxies at $z \lesssim 0.05$: since the redshift range covers a very small volume, the galaxy population is very likely to be largely contaminated by the outliers of photometric redshift estimates. To avoid this contaminating population, we employ the lower cutoff $z_{\text{ph,min}} = 0.1$ for our galaxy sample. Fig. 1 also shows that there are not many galaxies beyond $z = 0.9$. Furthermore, in order to study the impacts of low-redshift nonlinear structures and galaxy magnitude cut, we study the four galaxy catalogs listed in Table II. Note that the magnitude cut difference in the bright and faint samples are intended to study a possible contamination of imperfect galaxy-star separation.

Galaxy Sample	Magnitude range	z_{ph} range	\bar{n}_g [deg $^{-2}$] (NGH)	\bar{n}_g (SGH)	\bar{n}_g (NGH+SGH)	$\bar{n}_g(\text{SGH})/\bar{n}_g(\text{NGH})$
Bright-Shallow (BS) sample	$19.1 \leq m_i \leq 19.6$	$0.1 \leq z_{\text{ph}} \leq 0.4$	338.6	329.1	337.8	0.972
Bright-Deep (BD) sample	$19.1 \leq m_i \leq 19.6$	$0.1 \leq z_{\text{ph}} \leq 0.9$	502.4	501.7	502.3	0.999
Faint-Shallow (FS) sample	$19.6 \leq m_i \leq 20.1$	$0.1 \leq z_{\text{ph}} \leq 0.4$	453.1	431.1	451.2	0.951
Faint-Deep (FD) sample	$19.6 \leq m_i \leq 20.1$	$0.1 \leq z_{\text{ph}} \leq 0.9$	804.9	774.8	802.2	0.963

TABLE II: The definition of the four galaxy samples used in the analysis of this paper. The columns show the following: the i -band magnitude range imposed to define the galaxy sample; the photometric redshift range imposed to define the galaxy sample; the average number density of galaxies for the Northern Galactic hemisphere (NGH) region with area 6928 deg 2 ; the average number density for the Southern Galactic hemisphere (SGH) region with area 679 deg 2 ; the average number density for the whole NGH+SGH region with area 7607 deg 2 ; the ratio of the number densities of NGH and SGH regions.

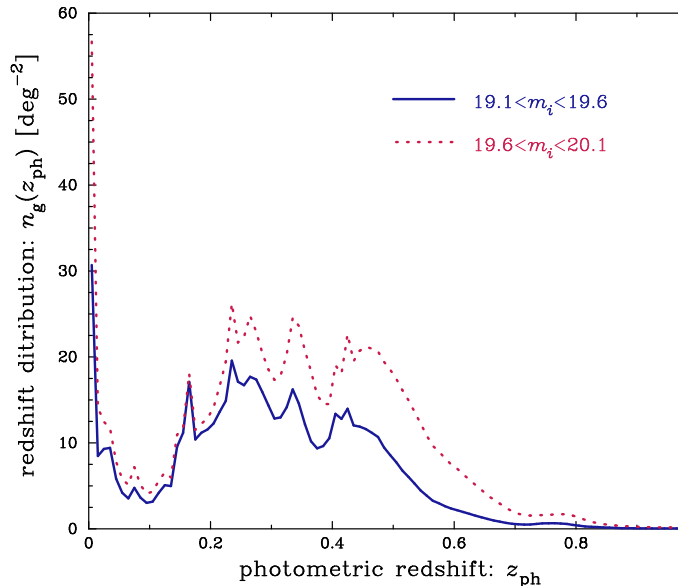


FIG. 1: The photometric redshift distribution ($0 \leq z \leq 1$) of galaxies used in this analysis, from the SDSS DR6 data. The solid curve shows the distribution for galaxies with i -band magnitude in the range $19.1 \leq m_i \leq 19.6$, while the dotted curve for $19.6 \leq m_i \leq 20.1$.

4. Constructing the galaxy number count field

Our method described in Sec. III is applicable to the pixelized data of galaxy distribution. For convenience, as done in [41], we employ the same pixelization as that used in the SFD dust extinction map, which is given in the format of pairs of 4096×4096 pixel Lambert projections, for each of the Northern and Southern Galactic hemispheres (hereafter NGH and SGH, respectively). Note that the pixel size is $(2'372)^2$ (see Appendix C in SFD). The SDSS galaxy distribution has a partial sky coverage, so we do not use the pixels that are not included in the survey region. Also for safety to avoid the pixelization effect, we do not use the pixels that reside at boundaries of the SDSS survey regions. For the remaining pixels, dust extinction effect on galaxy magnitudes is corrected for based on the SFD map, and then the galaxy number counts is computed in each pixel for each galaxy sample. However, since we are interested in the dipole (large-angular) anisotropy of galaxy distribution, we do not need small-scale clustering information. Therefore for computational convenience we create a coarser pixelized map of the galaxy counts in which each pixel is defined by combining 73×73 square-shape neighboring pixels. The area of each pixel (without masking) is 8.34 deg 2 . Furthermore, the SDSS regions contain masked regions as described before. Properly taking into account the masking effect, each pixel is assigned to the area of unmasked region and the combined galaxy number counts. Here for safety we do not use the pixels whose effective area is smaller than 10% of the pixel area after masking. As a result, the galaxy number counts we will work on are given in 983 and 168 pixels for the NGH and SGH regions, which have areas of 6928 and 679 deg 2 , respectively (1148 pixels with 7607 deg 2 in total).

Table II summarizes the average number density for the four galaxy catalogs. As mentioned in Sec. V A 3 above, we constructed the bright and faint samples to see effects of incomplete star-galaxy separation, expecting the faint

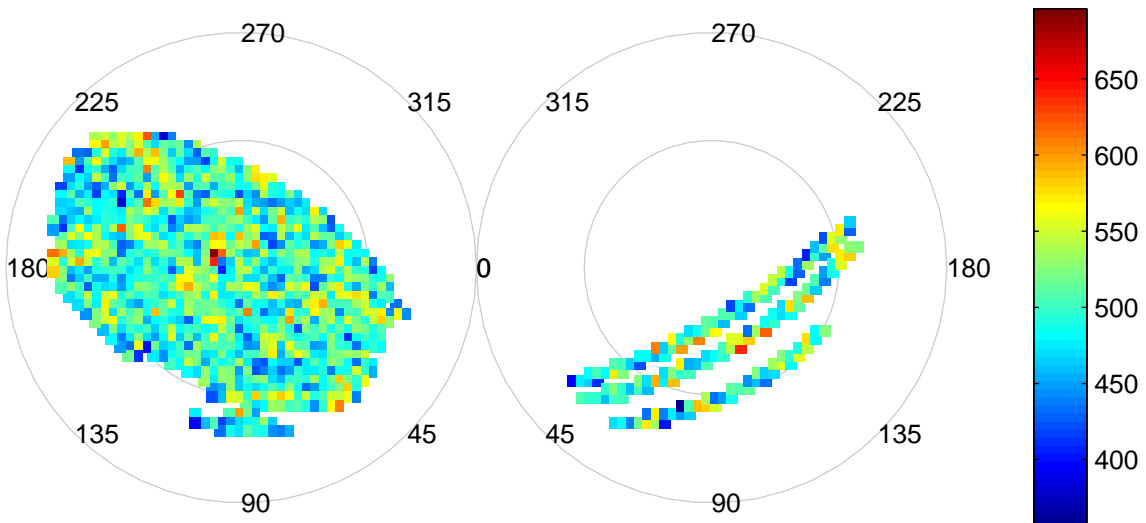


FIG. 2: The pixelized galaxy distribution of the BD sample in the Northern Galactic hemisphere (NGH: *left panel*) and the Southern Galactic hemisphere (SGH: *right*), respectively, based on the Lambert projection. The gray-color scales correspond to the number densities of galaxies in each pixel per unit square degrees as indicated by the right-side bar. In each panel the outer light-gray circle represents the zero galactic latitude ($b = 0^\circ$), while the inner circle $b = 45^\circ$. The numbers labeled along the $b = 0^\circ$ circle show the galactic longitudes.

samples suffer from more contamination. On the other hand, the shallow and deep samples are prepared to see effects of the large scale structure contamination, expecting the shallow samples have more contaminant. Other than these systematics, the average density of galaxies is found to be larger in the NGH region than in the SGH region. Although we are not sure for the significance due to the limited sky coverage of SDSS survey, the constraints on the aberration effect is found to be sensitive to an inclusion of the SGH region into the analysis as will be shown below, because the number density difference, if it is not real, mimics the dipole modulation of galaxy distribution.

Fig. 2 shows the pixelized galaxy distribution of the BD sample in the NGH (left panel) and SGH (right), respectively. The survey geometry can be clearly seen: the NGH region has a much greater coverage than the SGH, and the SGH regions have three survey stripes.

B. Computation of covariance matrix

The χ^2 -estimation of the aberration effect, given by Eq. (16), requires an estimate of the covariance matrix, \mathbf{C}_{ij} , where the indices i and j run over the pixels of galaxy density map.

As can be found from Eq. (17) the diagonal components, \mathbf{C}_{ii} , consist of two contributions: the Poisson noise arising due to discreteness of galaxy distribution and the sampling variance arising from the density fluctuations in large-scale structures. The Poisson noise contribution can be directly computed from the galaxy number counts in each pixel. On the other hand, the sample variance depends on the variances of galaxy density fluctuations of pixel scales, and the computation needs a few cares. Firstly, the areas of pixels are not uniform due to masking, and may vary from 0.834 to 8.34 deg^2 as described above. Secondly, a theoretical estimate of the sample variances (see Eqs. 18 and 19) involves several uncertainties: galaxy bias uncertainty and nonlinear clustering uncertainties corresponding to the pixel scales. In other words the linear mass fluctuations and the linear galaxy bias very likely break down on the relevant scales. Thus we instead estimate the sample variances directly from the SDSS galaxy catalog itself. To do this we used the original finest pixelized data of $(2.372)^2 \text{ arcmin}^2$ in order to estimate the variances as a function of the smoothing scales, where the smoothing is done by combining neighboring pixels of square-shape region. Note that the smoothing angular scale is simply estimated from the area of combined pixels as $\theta_{\text{sm}} = \sqrt{\Omega_{\text{pix}}/\pi}$.

Fig. 3 shows the estimated variances for the four galaxy samples over the entire SDSS survey region, where the variances are estimated for 18 different smoothing scales. We then assign the sample variance of an arbitrary pixel area by spline-interpolating the 18 data points. Thus we ignore the hole effect or pixel geometry due to masking for simplicity. Since the galaxy sampling region within each pixel in the galaxy catalog is not necessarily connected due to masking, the sample variance estimated in our method arises from the density fluctuations of the smallest

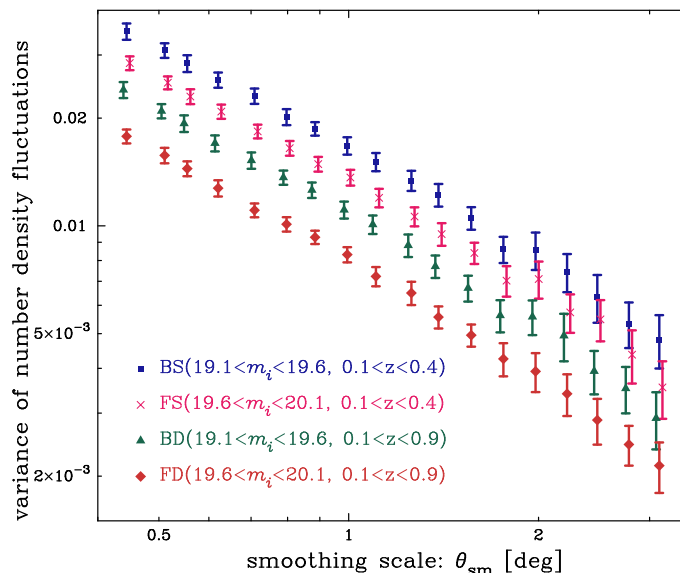


FIG. 3: The variances of galaxy number density fluctuations as a function of the smoothing scales, for the four galaxy catalogs defined in Table II. The variances are estimated from the pixelized galaxy catalogs with varying pixel sizes (here 18 different-size pixels are computed), and the smoothing scale in the horizontal axis is simply estimated from the pixel area as $\theta_{\text{sm}} = \sqrt{\Omega_{\text{pix}}/\pi}$ (see text for the details). Note that, for illustration purpose, the results for the FS and BD samples are slightly shifted in the horizontal direction. The error bars around each data points are estimated based on the bootstrap resampling method.

smoothing scales for a fixed area and would be greater than the actual sample variance. Thus our estimate of the sample variance is somewhat conservative.

Recall that, as given by Eq. (17), the Poisson noise contribution to the covariance is given by $1/(\bar{n}_g \Omega_{\text{pix}(i)})$ for a pixel with area $\Omega_{\text{pix}(i)}$ (\bar{n} is the average number density), where $\Omega_{\text{pix}(i)}$ varies from 0.834 to 8.34 deg^2 . Table II tells that, for our galaxy catalogs, the Poisson noise is in the range of $O(10^{-4}) - O(10^{-3})$. On the other hand, since the pixel areas in the range of 0.834 to 8.34 deg^2 correspond to the smoothing scales from 0.52 to 1.63 deg in Fig. 3, the sample variance is found to be $O(10^{-2})$. Therefore, for our galaxy catalogs, the sample variance dominates over the Poisson noise in the diagonal covariance components, more then by a factor 10, i.e. (samp. vari.) >10 (Poisson noise), thanks to the enormous size of SDSS galaxy catalog.

An estimate of the off-diagonal covariance components, $\mathbf{C}_{ij}(i \neq j)$, is more straightforward, where it contains only the sample covariance contribution. Since different pixels of our galaxy catalogs are separated by more than $2.89(\approx \sqrt{8.34})$ degrees, the cross-correlation between the galaxy density fluctuations of different pixels are safely considered to be in the linear regime. Therefore we use Eq. (18) to estimate the off-diagonal covariances. The computation requires several ingredients. For redshift projection, we used the photometric redshift distribution of galaxies in Fig. 1. As for the linear mass power spectrum we employed the transfer function given in [44] assuming the WMAP-3year cosmology [27]. As can be found from Eq. (18) the pixel window function is needed to specify; we adopted a top-hat type window function $W(\boldsymbol{\theta}) = 1/(\pi\theta_{\text{th}}^2)$ where θ_{th} is simply estimated from the pixel area as $\theta_{\text{th}} = \sqrt{\Omega_{\text{pix}(i)}/\pi}$ [61]. Finally we also need to specify the linear bias parameter of each galaxy sample, b_g . We estimated b_g by fitting the variances at large angular scales $1.5^\circ \leq \theta \leq 2.6^\circ$ to the linear theory predictions, resulting in the linear bias parameters $b_g \simeq 1.0$ for both the BS and FS sample galaxies, while $b_g \simeq 1.2$ for the BD and FD samples.

C. Expectation

Before going to the results, the upper panel of Fig. 4 shows the expected dipole modulation pattern of galaxy distribution in the SDSS survey region, *if* the aberration effect on the SDSS galaxy distribution is in the same amplitudes and angular direction as in the CMB dipole, i.e. if the Earth's peculiar velocity to the SDSS galaxy distribution is $\beta_{\text{CMB}} = 1.231 \times 10^{-3}$ in the direction $(l_{\text{CMB}}, b_{\text{CMB}}) = (264^\circ 31', 48^\circ 05')$ in the Galactic coordinates.

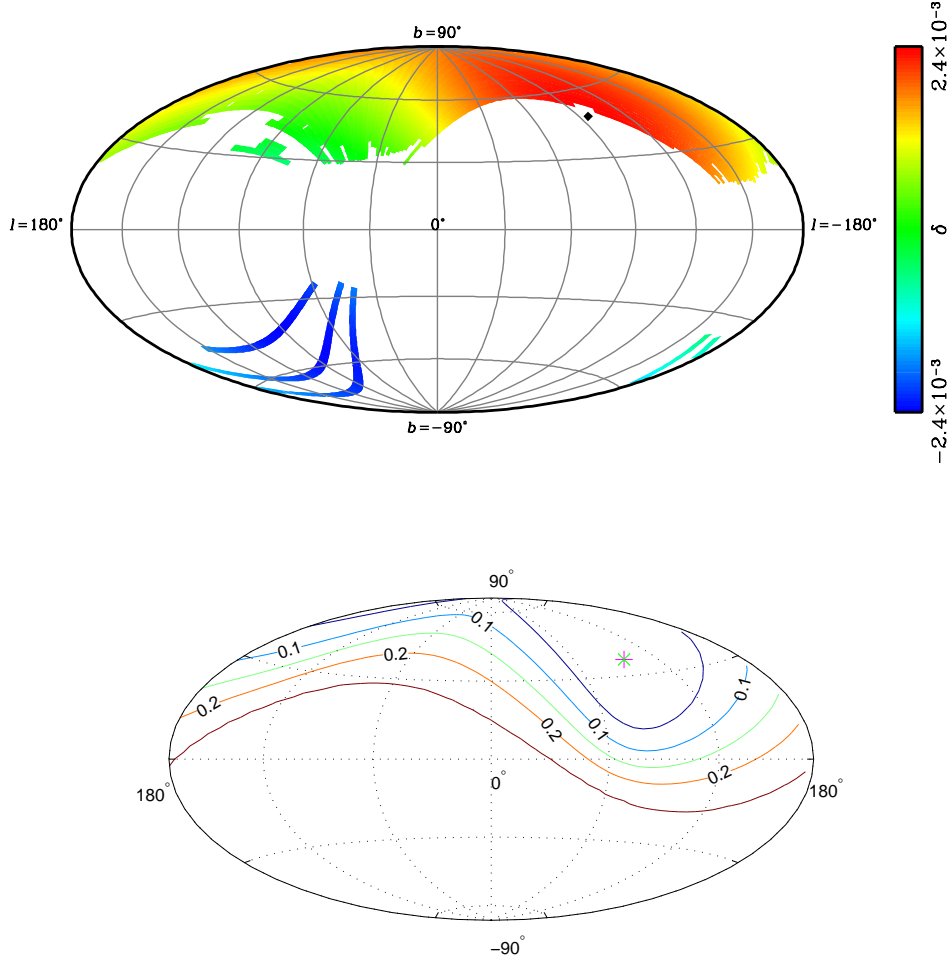


FIG. 4: *Upper panel:* An expected dipole pattern of the galaxies number density field for the SDSS survey region. Here we assumed the dipole amplitude and direction as those of the CMB dipole: the velocity amplitude $\beta = 1.231 \times 10^{-3}$, and the angular direction is denoted by the black square symbol. We set $\tilde{\beta} = \beta$ in Eq. (9) for simplicity. The color scales denote the number density fluctuations of galaxies as indicated by the right-hand color bar. *Lower panel:* The expected accuracy of constraining the dipole angular direction by the χ^2 fitting (Eq. 16 or 27), where the covariance matrix for the FD sample is used as a representative example. The contours denote the $\langle \Delta\chi^2 \rangle$ distribution over the sky, and show that the angular direction is not constrained: all the directions are within the 1σ region ($\langle \Delta\chi^2 \rangle \leq 2.3$ for two parameter case). The cross and the plus symbols indicate the χ^2 minimum and the CMB dipole direction, respectively. The $\langle \Delta\chi^2 \rangle$ value corresponding to each contour line is indicated by the numbers on the line.

For simplicity we ignore the Doppler effect, i.e., set $\tilde{\beta} = \beta$ in Eq. (9). The plot shows the $O(10^{-3})$ -level density modulation can be expected, however, the partial sky coverage of the SDSS region seems to significantly obscure the characteristic pattern and prevent the detection. It may also be worth noting that the CMB dipole direction predicts a negative number density contrast in the SGH region, which may be indicated from our galaxy catalogs as shown in Table II, although it may be just a coincidence.

Assuming the dipole density modulation shown in the upper panel of Fig. 4, we then compute the mean χ^2 values (minus the degrees of freedom, or “d.o.f.”) with varying free parameters ($\hat{\mathbf{v}}, \tilde{\beta}$). In other words, using Eq. (16) we

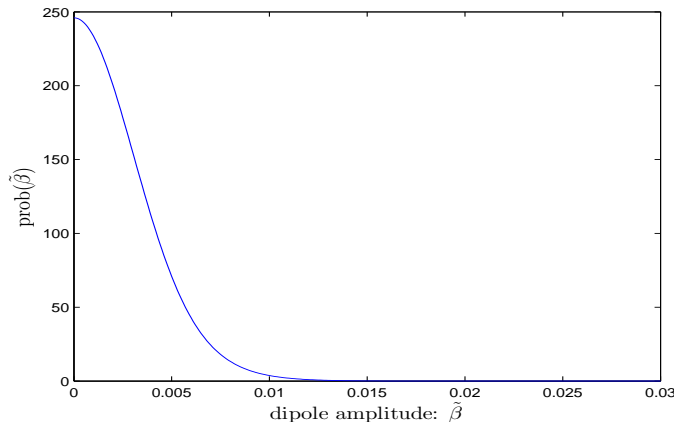


FIG. 5: An expected marginalized likelihood of the dipole amplitude $\tilde{\beta}$ is shown for the SDSS galaxy distribution depicted in Fig. 4. The SDSS catalog allows for an accuracy of $\tilde{\beta} = O(10^{-2})$ for the aberration effect search.

compute

$$\begin{aligned} \langle \Delta\chi^2(\hat{\mathbf{v}}, \tilde{\beta}) \rangle &\equiv \langle \chi^2(\hat{\mathbf{v}}, \tilde{\beta}) \rangle - (\text{d.o.f}) \\ &= \sum_{i,j=1}^{N_{\text{pix}}} \left[\langle \delta_{\text{assumed}}(\boldsymbol{\theta}_i) \rangle - \delta_{\text{model}}(\boldsymbol{\theta}_i; \hat{\mathbf{v}}, \tilde{\beta}) \right] [\mathbf{C}]_{ij}^{-1} \left[\langle \delta_{\text{assumed}}(\boldsymbol{\theta}_j) \rangle - \delta_{\text{model}}(\boldsymbol{\theta}_j; \hat{\mathbf{v}}, \tilde{\beta}) \right], \end{aligned} \quad (27)$$

where $\langle f \rangle$ denotes an ensemble average of the quantity f and

$$\langle \delta_{\text{assumed}}(\boldsymbol{\theta}_j) \rangle = 2\beta_{\text{CMB}} \hat{\mathbf{v}}_{\text{CMB}} \cdot \boldsymbol{\theta}_j. \quad (28)$$

(By subtracting the degrees of freedom, this quantity becomes zero when our free parameters $(\hat{\mathbf{v}}, \tilde{\beta})$ coincide with the hypothetical observation parameters $(\hat{\mathbf{v}}_{\text{CMB}}, \beta_{\text{CMB}})$ in this case). The survey geometry of the SDSS DR6 are taken into account when computing $\boldsymbol{\theta}_j$, the covariance matrix and δ_{model} .

The lower panel of Fig. 4 then gives a more quantitative estimate, showing the accuracy of determining the dipole angular direction from the expected number density modulation. To be more explicit, this plot shows the theoretically expected mean χ^2 difference between the best-fit model and models with varying model parameters to specify the angular direction of the peculiar velocity, marginalized over the velocity amplitude computed from Eq. (27): $\langle \Delta\chi^2(l, b) \rangle$. We used the covariance matrix for the FD galaxy sample (see Sec. VB) in order to compute the $\Delta\chi^2$. The figure clearly shows that $\langle \Delta\chi^2 \rangle$ is smaller than 1 over the entire sky. That is, the aberration effect is very difficult to detect, if the peculiar velocity to the SDSS galaxy is similar to the CMB dipole amplitude. In other words, the covariance, especially the intrinsic galaxy clustering contamination, is so significant compared to the aberration effect. This result is consistent with a rough estimate shown in Table I. Fig. 5 shows the marginalized probability distribution of the dipole amplitude parameter $\tilde{\beta}$. Only an upper limit on $\tilde{\beta}$ at the level $\tilde{\beta} \lesssim 10^{-2}$ is likely to be obtained from the SDSS catalog.

D. Results

Now let us move on to the measurement results. Here in the analysis on the real data, we first count number of galaxies in each pixel and compute the density perturbation field using Eq. (12). Second, choosing model parameters $(\hat{\mathbf{v}}, \tilde{\beta})$, we compute δ_{model} using Eq. (15) and construct $\chi^2(\hat{\mathbf{v}}, \tilde{\beta})$ using Eq. (16) for those particular model parameters. Varying the model parameters, we iterate the second step, searching for the parameters that minimize the χ^2 value. The value of $\tilde{\beta}$ is varied in the range of $0 \leq \tilde{\beta} \leq 7.0 \times 10^{-2}$ and the values of (l, b) are varied over the entire sky directions. We used the covariance matrix computed based on the method in Sec. VB for each galaxy sample.

Table III summarizes the χ^2 -fitting results for the four galaxy samples listed in Table II. The second- and third-columns in the table give the minimum χ^2 value, χ_{min}^2 , for the best-fit model and its model parameters. The fact $\chi^2 \approx (\text{pixel number})$ implies that our covariance matrix estimate is reasonable. The table shows that the best-fit values of $\tilde{\beta}$ are of the order of $O(10^{-2})$ as expected from Fig. 5. Table III also shows the χ^2 -differences, $\Delta\chi^2$, obtained

Galaxy Sample	χ^2_{\min}	best-fit model: (β, l, b)	Errors: $(\Delta\beta, \Delta\theta)$	$\chi^2_{\text{CMB}} - \chi^2_{\min}$	$\chi^2_{\beta=0} - \chi^2_{\min}$
BS sample	1080.3	$(0.0127, 310^\circ, 30^\circ)$	$(+0.0067, 64^\circ)$ $(-0.0054, 64^\circ)$	5.85	7.22
BD sample	1211.4	$(0.0087, 290^\circ, -10^\circ)$	$(+0.0059, 100^\circ)$ $(-0.0057, 100^\circ)$	2.01	2.35
FS sample	1108.0	$(0.0156, 290^\circ, 60^\circ)$	$(+0.0039, 40^\circ)$ $(-0.0034, 40^\circ)$	18.7	21.7
FD sample	1288.1	$(0.0121, 280^\circ, 75^\circ)$	$(\pm 0.0023, 33^\circ)$	21.2	25.6

TABLE III: The results for the χ^2 fitting for the four SDSS galaxy samples defined in Table II. The second column labeled as “ χ^2_{\min} ” denotes the minimum χ^2 value for the best-fit model, and the third column gives the best-fit parameters. The fourth column shows, for each sample, the 1σ error for $\tilde{\beta}$ and the 1σ uncertainty of determining the dipole direction in radius from the best-fitting angular position. The fifth column gives the χ^2 -difference between the best-fit model and the case that the peculiar motion induced dipole has the same amplitude and angular direction as those of the CMB dipole, given as $(\beta_{\text{CMB}}, l_{\text{CMB}}, b_{\text{CMB}}) = (1.231 \times 10^{-3}, 264^\circ.31, 48^\circ.05)$. The sixth column shows the χ^2 -difference compared to no aberration effect case, $\beta = 0$.

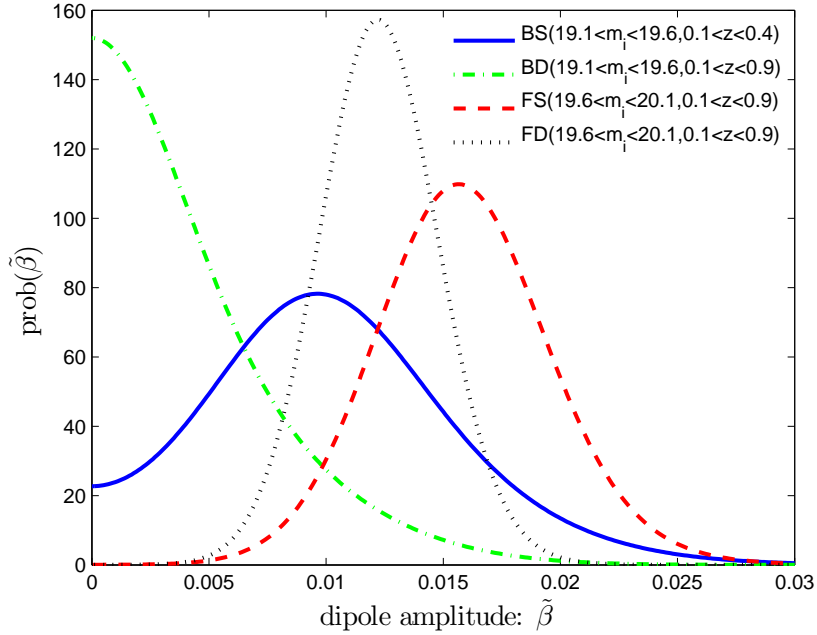


FIG. 6: The likelihood probability distribution for the dipole amplitude parameter $\tilde{\beta}$ of the aberration effect, marginalized over the angular direction parameters (l, b) , for the four galaxy samples. The FS and FD samples which preferentially include fainter galaxies prefer a non-zero $\tilde{\beta}$ with the amplitudes $O(10^{-2})$. The other two samples are consistent with zero $\tilde{\beta}$.

by comparing the χ^2_{\min} with two models: one assumes the CMB dipole amplitude and direction for the aberration effect, and the other is no aberration effect ($\beta = 0$). For both cases, the χ^2 differences are modestly large, except for the BD sample, implying that the dipole angular modulation pattern, which is not necessarily the aberration effect, is marginally detected.

Fig. 6 is the marginalized probability distribution of the dipole amplitude parameter $\tilde{\beta}$ for the four galaxy samples. The FS and FD samples seem to prefer non-zero $\tilde{\beta}$, however, the likely amplitude is $O(10^{-2})$, implying that the peculiar velocity of the Earth relative to the SDSS galaxy distribution is $v \sim 3000 \text{ km s}^{-1}$. Such a large peculiar velocity is difficult to explain in the currently concordance ΛCDM model, and therefore we believe this is likely due to either the intrinsic galaxy clustering contamination or unresolved systematic effects, or both, as also demonstrated in Figs. 4 and 5. We will come back to this issue later in this section.

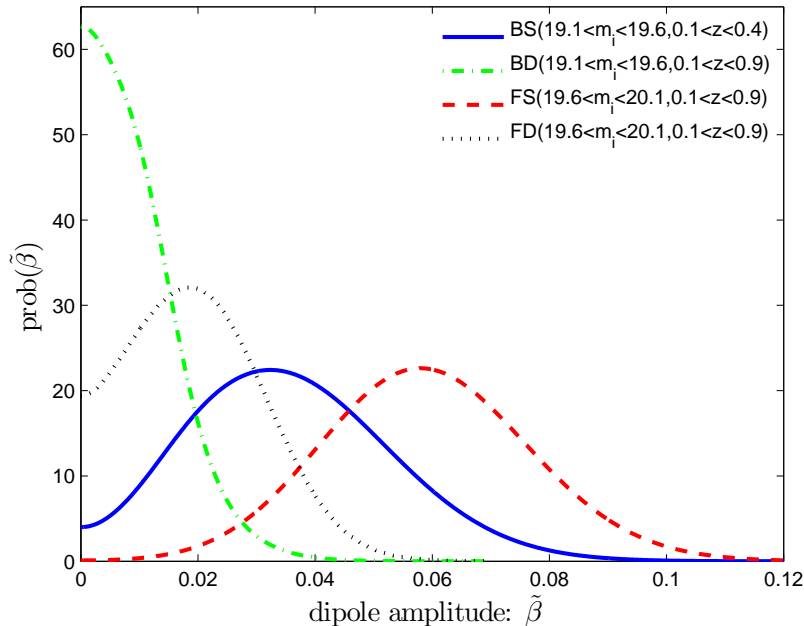


FIG. 7: Estimated marginalized probability of the dipole amplitude $\tilde{\beta}$, where only the data in the Northern Galactic hemisphere region is used.

Fig. 8 shows how the $\Delta\chi^2$ value, marginalized over the dipole amplitude parameter $\tilde{\beta}$, varies as a function of the peculiar velocity directions on the sky. It would be interesting to find that the method developed here can constrain the velocity directions. Again, for the FS and FD cases, the dipole directions are constrained at more than 3σ level ($\Delta\chi^2 = 11.8$). Also interestingly, the preferred dipole direction is close to the CMB dipole direction. If a possible detection of the galaxy dipole is due to the intrinsic clustering contamination, the inferred direction is not necessarily similar to the CMB direction since we have removed the contamination due to the nearby large scale structures using the photometric redshift information.

Now let us discuss possible causes of the indicated dipoles in our samples other than the BD sample. We construct the four galaxy catalogs to study possible remaining systematic effects due to the star-galaxy separation and the intrinsic clustering contamination, as are defined in Table II. As shown in Table III and Fig. 8, the “faint” samples, which are supposed to be more contaminated by an imperfect star-galaxy separation than for the “bright” samples, tend to prefer the dipole directions at higher galactic latitudes. This is counter-intuitive, because the faint samples may suffer from more star contamination towards lower galactic latitudes, which in turn causes the dipole direction in the lower latitudes due to the enhanced overdensity. Hence the imperfect star-galaxy separation seems not a main source of the systematic effects. On the other hand, if comparing the “deep” and “shallow” samples, the shallower sample is supposed to be more affected by the intrinsic galaxy clustering contamination from more evolving nonlinear structures at lower redshifts, if the photometric redshifts are well reliable. In fact Fig. 6 shows that the dipole amplitudes tend slightly larger for shallower samples.

Another concern arises from the partial sky coverage. In particular, as discussed in Table II, the SDSS galaxy samples tend to have a smaller average number density in the Southern Galactic hemisphere than in the Northern Galactic hemisphere, which may cause an (apparent) dipole anisotropy. Fig. 7 shows the probability distribution of $\tilde{\beta}$ if only the NGH region is used in the analysis. Now all four samples show broader distributions, and all but FS sample are consistent with zero $\tilde{\beta}$. Fig. 9 shows the same plots as Fig. 8, but here again we have excluded the data in the Southern Galactic hemisphere from our four samples in the analysis. The 1σ contours in the four plots become smaller, indicating larger dipole amplitudes as consistent with the finding on Fig. 7 above. We also note that the minimum χ^2 values of all four samples (green crosses in Fig. 9) more or less tend to move toward the Northern Galactic pole than in Figs. 8. Hence the number density differences between NGH and SGH does move the direction of the detected dipoles in all the four samples toward the CMB dipole direction, yet the origin of the difference itself is unknown. As far as direction is concerned, the aberration induced dipole expected from the CMB dipole does predict

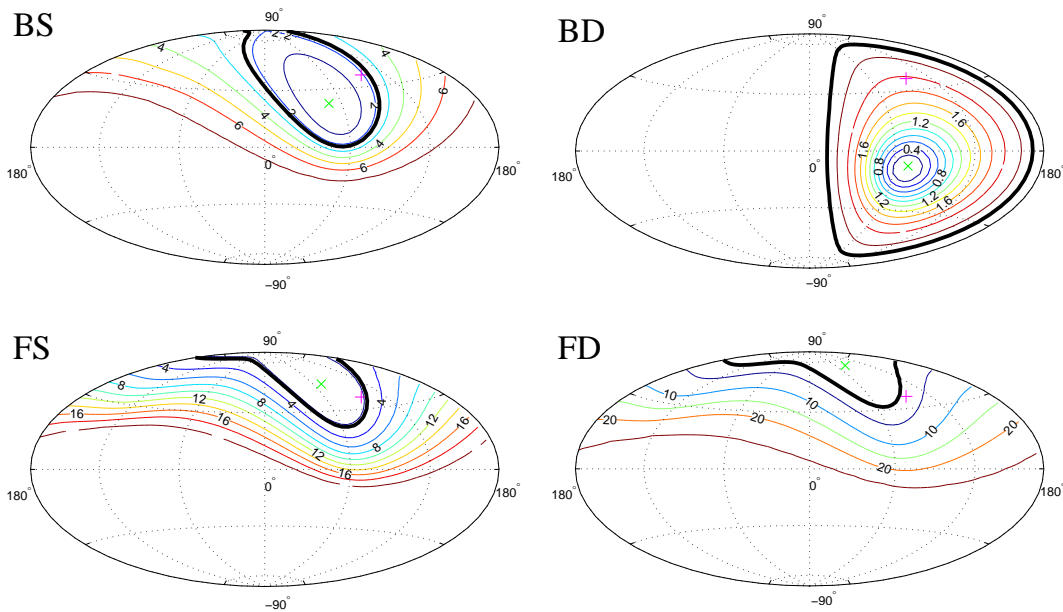


FIG. 8: The $\Delta\chi^2$ distribution as a function of the dipole direction parameters (l, b) on the sky, marginalized over the dipole amplitude parameter $\tilde{\beta}$. The upper-left, upper-right, lower-left and lower-right panels are the results for the BS, BD, FS, and FD samples, respectively. The thick (black) contour corresponds to the 1σ uncertainty region ($\Delta\chi^2 = 2.3$). The ‘x’ symbol denotes the best-fit direction, while the ‘+’ symbol denotes the CMB dipole direction, $(l_{\text{CMB}}, b_{\text{CMB}}) = (264^\circ.31, 48^\circ.05)$.

such a difference between NGH and SGH as is indicated in the upper panel of Fig. 4. A data having a wider sky coverage, such as LSST, is desired to settle down this issue.

The reason for all but BD samples, when excluding the SGH data, show the minimum χ^2 values around the Northern Galactic pole may be attributed to imperfect Galactic dust extinction correction, although it is not perfectly clear how Galactic dust can produce the difference in the BS and BD samples (or, in other words, how effects of Galactic dust differ among different redshifts). In this paper we have assumed that the dust extinction correction by the SFD dust map is perfect, but it is well-known in the literature (see, e.g., [41]) that there may remain some residual systematics in the map. In summary, since the BD sample with and without the data in the SGH, which is the most robust sample against possible systematics among our four samples, indicates zero dipole, we conclude that the aberration effect is not detected from the SDSS DR6 in our analysis.

VI. PROSPECT FOR A FUTURE WIDE-AREA SURVEY: LSST

As we have so far shown, a survey with large sky coverage and sufficiently deep redshift coverage is required to detect the aberration effect. The planned galaxy survey, the Large Synoptic Survey Telescope (LSST) [45, see also <http://www.lsst.org/>], will provide us with a most promising opportunity to explore the aberration effect. Here we estimate the expected accuracy.

To estimate the forecasts, we need to specify survey parameters. According to [46], the survey area is assumed to be 18863 deg^2 , and the survey geometry is restricted to the region $-75^\circ \leq \delta \leq 15^\circ$, excluding the galactic disk region of $-15^\circ \leq b \leq 15^\circ$ (also see the figure below). For the galaxy redshift distribution, we simply assume the analytic form given by Eq. (4) in [47]:

$$n_g(z) \propto z^2 e^{-z/z_0} \quad (29)$$

with $z_0 = 0.4$, which has the mean redshift $\bar{z} = 1.2$. The galaxy distribution is normalized so as to have the mean number density of galaxies of 50 per unit square arcminutes [47]. The assumed LSST galaxy redshift distribution is shown in Fig. 10 along with the ones for the SDSS samples shown in Fig. 1.

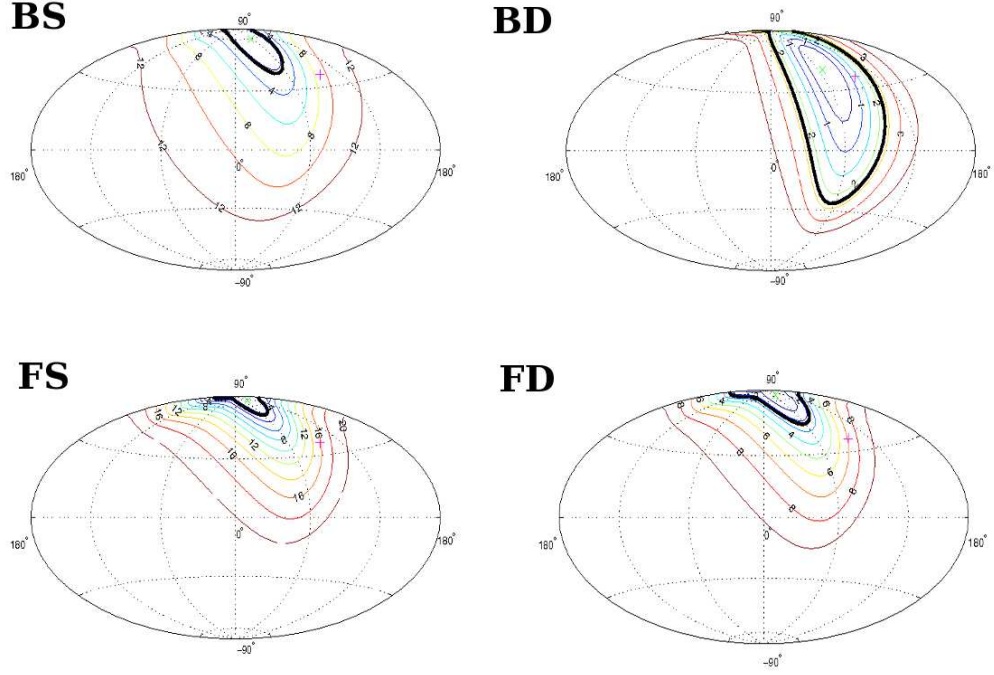


FIG. 9: The same as Fig. 8, but here for these plots, we have used the SDSS DR6 data in the Northern Galactic hemisphere only.

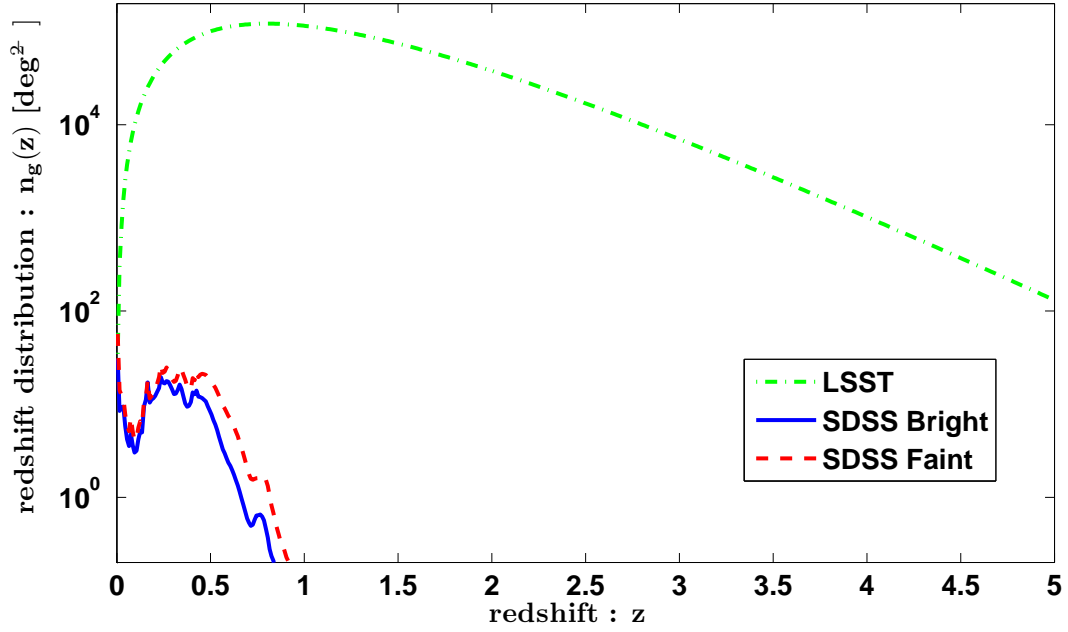


FIG. 10: The expected redshift distribution $n_g(z)$ of the LSST survey (dash-dotted line). The mean angular number density of 50 per unit square arcminutes is assumed [47]. Also shown for comparison are the galaxy redshift distribution of the SDSS bright sample $19.1 < m_i < 19.6$ (solid line) and of the SDSS faint sample $19.6 < m_i < 20.1$ (dashed line).

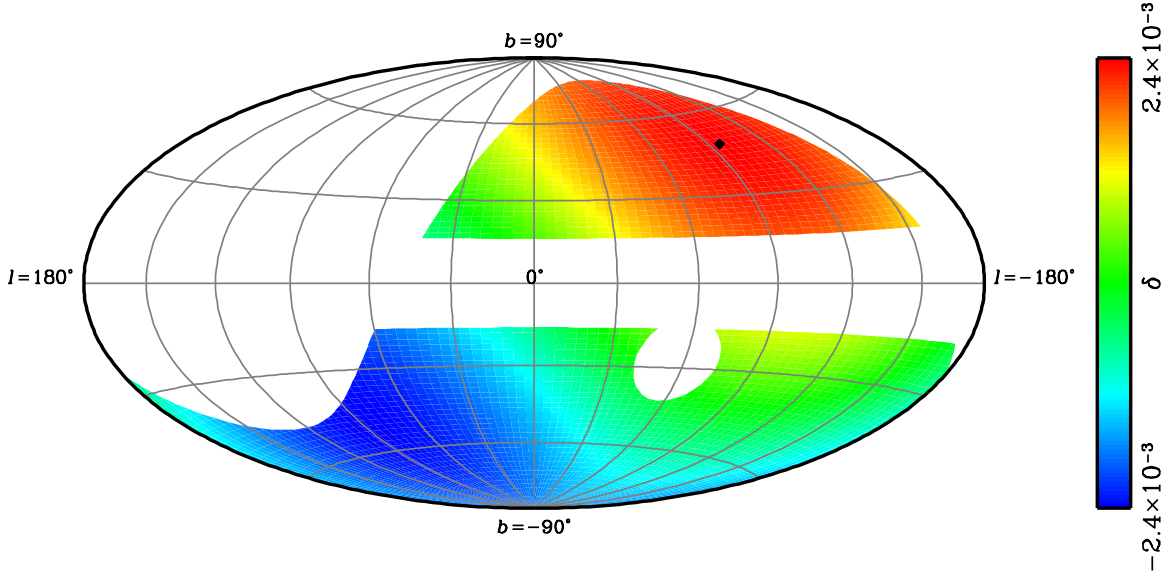


FIG. 11: The expected dipole pattern of the galaxies number density field expected for a hypothetical LSST-like survey, assuming the CDM dipole amplitude and direction as in Fig. 4. The diamond symbol indicates the CMB dipole direction.

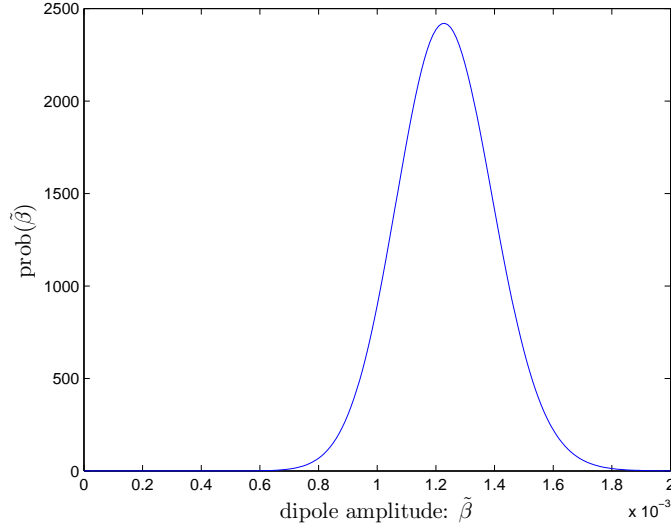


FIG. 12: The expected marginalized probability of the dipole amplitude parameter $\tilde{\beta}$ for the aberration effect on the LSST galaxy distribution in Fig. 11.

Fig. 11 shows the expected dipole anisotropy pattern in the LSST galaxy distribution, assuming the CMB dipole amplitude and directions. (For simplicity, we ignore the Doppler effect, i.e., set $\tilde{\beta} = \beta$ in Eq. (9) to produce the figures in this section.) It is clear that the wide sky-coverage can nicely capture the dipole pattern.

To quantify the detectability of the aberration effect with the LSST, we need to model the sample variance contribution to the covariance matrix. We first considered the pixelized map with 213 pixels; each pixel has an area of

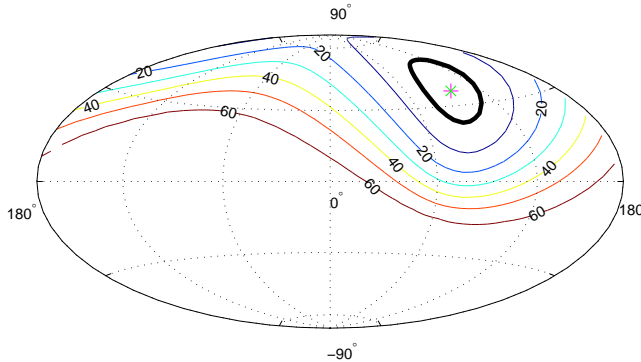


FIG. 13: The expected mean $\Delta\chi^2$ (i.e., $\langle\Delta\chi^2\rangle$ given by Eq. (27)) distribution for the LSST survey. The contours are stepped by $\langle\Delta\chi^2\rangle = 10$, while the thick contour denotes the 1σ region. The 1σ accuracy of determining the angular dipole direction is ~ 20 degrees in radius.

88 square degrees or ~ 10 degrees scale. The pixel size is sufficiently large, so we use the linear theory to compute the sample variance contributions. However, to reduce the intrinsic clustering contamination from structures at low redshifts, we only include galaxies at redshifts greater than $z = 1$. Also we assume the linear bias parameter $b_g = 1$ for simplicity.

Figs. 12 and 13 show the forecasts, which show the marginalized probability of the $\tilde{\beta}$ parameter estimation and the expected mean $\Delta\chi^2$ distribution over the sky, respectively. From both the plots, it is clear that the LSST may allow for a significant detection of the aberration effect: the accuracy of the $\tilde{\beta}$ parameter estimation is at a level of $\sigma(\tilde{\beta}) = 10^{-4}$, while the dipole directions can be determined with the precision of 20 degrees in radius. If we can have a full-sky survey with similar depth to the LSST, the ultimate precision is 10 degrees in radius.

VII. SUMMARY AND DISCUSSION

In this paper we have used the SDSS DR6 galaxy catalog to explore the dipole anisotropy pattern in the angular galaxy distribution caused by the aberration effect due to the Earth’s peculiar motion to the matter rest-frame. The SDSS DR6 catalog, which covers about 8000 square degrees, allows us to construct the currently most reliable galaxy catalog for our purpose because the data has well-calibrated, homogeneous and secure photometric and astrometric properties.

After developing a method to explore the aberration effect signal (see Sec. III), we estimated the detectability of the dipole signal for SDSS- and LSST-type surveys assuming the CMB dipole amplitude and the concordance Λ CDM model properly taking into account the contamination effects (Sec. IV). We found that the intrinsic galaxy clustering at low redshifts gives a significant contamination. Recalling that for a CDM model the galaxy distribution has greater inhomogeneities at smaller scales, the small-scale galaxy distribution at lower redshifts is viewed by an observer with larger angles, and the strong inhomogeneities significantly obscure the aberration effect if the Earth’s peculiar motion to the matter rest-frame is similar to that for the CMB dipole amplitude, i.e. $\tilde{\beta} = O(10^{-3})$. In other words, the dipole anisotropy due to the intrinsic clustering can be greater than the aberration effect for a low-redshift galaxy catalog. The Poisson contamination due to the discrete galaxy distribution is smaller, but not negligible even with such a huge number of SDSS galaxies. Therefore our results imply that the previous report on a possible detection of the aberration effect may be due to these contaminating effects (see also [48]).

To remove the contaminating effect of the low-redshift galaxies as much as possible, we used the photometric redshift information to define a secure catalog of galaxies. We considered the four galaxy catalogs to study possible remaining systematic effects due to the star-galaxy separation and the intrinsic clustering contamination, as are defined in Table II. As shown in Table III and Fig. 8, the “faint” samples, which are supposed to be more contaminated by an imperfect star-galaxy separation than for the “bright” samples, tend to prefer the dipole directions at higher galactic latitudes. This is counter-intuitive, because the faint samples may suffer from more star contamination towards lower galactic

latitudes, which in turn causes the dipole direction in the lower latitudes due to the enhanced overdensity. Hence the imperfect star-galaxy separation seems not a main source of the systematic effects. We also compared the “deep” and “shallow” samples by using the photometric redshift information. As described above, the shallower sample is supposed to be more affected by the intrinsic galaxy clustering contamination from more evolving nonlinear structures at lower redshifts. However, the dipole directions for both the deep and shallow samples are found to be similar, which indeed prefers a direction around the CMB dipole direction within the $1\text{-}\sigma$ region, except for the “faint-deep” sample (see Fig. 8).

Among the four galaxy catalogs, the “faint-deep” and “faint-shallow” samples are found to give a possible detection of dipole amplitude given as $\beta \sim 10^{-2}$ corresponding to the peculiar velocity $v \sim 3000\text{km s}^{-1}$ (see Fig. 6). These values are significantly larger than the CMB dipole amplitude by a factor 10. The peculiar velocity amplitude of 10^3km s^{-1} is similar to the virial velocities of a massive cluster, however, we know our Galaxy is not in such a cluster. On the other hand, the large-scale (relative) bulk flow of 1000km s^{-1} is at $2 - 3\sigma$ deviations from the typical peculiar velocity of 470km s^{-1} predicted by the standard ΛCDM structure formation model. Furthermore, the previous studies on the peculiar velocity field for the Local Group have not found such a large peculiar velocity. Therefore we believe that a possible indication on the aberration effect on the SDSS galaxy distribution is not significant, and may be due to residual contaminating effects.

We argued that the dipole direction may be caused, at least partly, by the apparent systematic difference of galaxy number densities between the SDSS survey regions of the Northern and Southern Galactic hemispheres (NGH and SGH, respectively), where the SGH region has a smaller average number density than the NGH (see Table II). We found that the number density differences between NGH and SGH does move the direction of the detected dipoles in all the four samples toward the CMB dipole direction, however, the origin of the difference itself is unknown. The two regions are separated, and the SGH region has a much smaller sky coverage (679 deg^2) compared with the NGH region (6928 deg^2). A data having a wider sky coverage is desired to settle if this difference is real or due to some systematics in our analysis.

Another concern is on the Galactic dust extinction correction. Indeed, when excluding the SGH data, the preferred dipole directions of all samples more or less move toward the Northern Galactic pole. Hence we suspect that Galactic dust may cause one part of our detection of the dipoles in the three less robust samples other than the BD sample (another possible part is the number density difference between NGH and SGH). Although we have assumed in this paper that the SFD dust map [42] gives us a perfect dust extinction correction, Yahata et al. [41] pointed our remaining systematics in low dust extinction regions in the map. Therefore an indication of the dipole anisotropy we found is not yet conclusive.

We quantitatively showed that a survey with almost full-sky coverage and sufficient depth is ideally needed to explore the aberration effect on the galaxy distribution. Future surveys, Pan-Starrs [49, see also <http://pan-starrs.ifa.hawaii.edu/public/>] or LSST [45], are such a survey and offer a chance to explore the signal. In this paper we showed that LSST may allow for a significant detection of the aberration effect. Even for the effect similar to the CMB dipole amplitude, the angular direction of the aberration effect can be determined with precision of 20 degrees in radius. If the cosmic bulk flow of order $\sim 1000\text{km s}^{-1}$ implied in Kashlinsky et al. (2008)[50] extends out to the horizon and therefore we are at rest in the matter rest-frame, the LSST survey will provide us a good opportunity for either accepting or rejecting such a bulk flow. Thus LSST may offer a unique chance to constrain the horizon-scale perturbations where some exotic physics related to cosmic acceleration such as dark energy and super-void may play a role.

There are other methods/data-sets that allow to explore the horizon-scale peculiar velocity field relative to the Earth’s motion. For instance, using a homogeneous catalog of quasars, such as that of SDSS, is advantageous to reduce the intrinsic clustering contamination due to the higher redshift coverage. However a clean identification of quasars from stellar population from imaging data is always problematic. Also the Poisson noise can be significant due to a much smaller number density of quasars.

Another interesting method is using the kinetic Sunyaev-Zel’dovich (SZ) effect that is caused by the peculiar velocities of ionized medium that scatters off CMB photons causing the secondary temperature fluctuations by the Doppler shift. For example, the kinetic SZ effect can be extracted by measuring the CMB fluctuations. The advantage of this method is it allows to directly measure the line-of-sight component of peculiar velocity at the cluster redshift. In fact there are several attempts to measure the kinetic SZ effect by stacking the CMB fluctuations in the sky regions of clusters in order to explore the excess in the temperature fluctuations [50–52]. In particular, Kashlinsky et al. (2008)[50] reported a possible significant detection of the large-scale bulk flow of X -ray luminous clusters, implying the bulk flow of $\sim 1000\text{km s}^{-1}$, apparently similar to that indicated from our analysis on our faint samples within the uncertainties, in the angular direction not far from the CMB dipole direction (also see [53, 54]). Based on this surprising result, it was speculated that the large-scale bulk flow may originate from the non-standard horizon-scale perturbations, for example the tilt across the observable Universe due to the pre-inflationary inhomogeneities [16]. This result is, very interesting though, still under debate, and a further analysis will be needed by using a homogeneous

massive sample of clusters. Moreover, a high-angular-resolution and high-sensitive CMB measurement has a potential to extract the kinetic SZ effect due to the ionized intergalactic medium (more exactly known as the Ostriker-Vishniac effect [55]). Thus it would be worth exploring large-scale bulk flow of the Universe by combining various methods in order to explore the possible new horizon-scale physics, which is very difficult to explore by other means.

Acknowledgments

We would like to thank Masashi Chiba, Yuji Chinone, Makoto Hattori, Nobuhiro Okabe, Tsutomu T. Takeuchi, Anže Slosar, and Saleem Zaroubi for useful comments that clarifies statistical issues in our analysis. We are grateful to Ryuichi Takahashi and Guilhem Lavaux who let us know a couple of interesting references. We thank the anonymous referee who carefully read our manuscript and gave us interesting comments. We have used the FFTLog code (<http://casa.colorado.edu/~ajsh/FFTLog/>) written by professor Andrew Hamilton to whom we are grateful. K. Y. was supported by Grants-in-Aid for Japan Society for the Promotion of Science Fellows. Y. I. was supported by a Grant-in-Aid for the 21st Century Center of Excellence (COE) Program “Exploring New Science by Bridging Particle-Matter Hierarchy” and is supported by the Japan Society of the Promotion of Science Global COE Program (G01): “Weaving Science Web beyond Particle-Matter Hierarchy”, both in Tohoku University, and both funded by the Ministry of Education, Science, Sports and Culture of Japan. Funding for the SDSS and SDSS-II has been provided by the Alfred P. Sloan Foundation, the Participating Institutions, the National Science Foundation, the U.S. Department of Energy, the National Aeronautics and Space Administration, the Japanese Monbukagakusho, the Max Planck Society, and the Higher Education Funding Council for England. The SDSS Web Site is <http://www.sdss.org/>. The SDSS is managed by the Astrophysical Research Consortium for the Participating Institutions. The Participating Institutions are the American Museum of Natural History, Astrophysical Institute Potsdam, University of Basel, University of Cambridge, Case Western Reserve University, University of Chicago, Drexel University, Fermilab, the Institute for Advanced Study, the Japan Participation Group, Johns Hopkins University, the Joint Institute for Nuclear Astrophysics, the Kavli Institute for Particle Astrophysics and Cosmology, the Korean Scientist Group, the Chinese Academy of Sciences (LAMOST), Los Alamos National Laboratory, the Max-Planck-Institute for Astronomy (MPIA), the Max-Planck-Institute for Astrophysics (MPA), New Mexico State University, Ohio State University, University of Pittsburgh, University of Portsmouth, Princeton University, the United States Naval Observatory, and the University of Washington.

Appendix A: Dipole Amplitudes

This appendix briefly explains a method of estimating the amplitudes of the expected dipole moments in the galaxy density fluctuation field from three contributions: the Poisson shot noise, the large scale structure, and the motion of us (the Earth) with respect to the CMB rest frame. This method is used in Sec. IV to obtain a rough estimate of a signal to noise ratio for detecting a dipole modulation. We first consider the case of a hypothetical all-sky survey, then a partial-sky survey. We follow the method of [36, 37, 56] with which readers’ may consult for further details.

1. All-Sky Survey

This section considers a hypothetical all-sky survey and we will start with our definitions of the dipole moments. For a galaxy number density field $n(\boldsymbol{\theta})$, we compute a spherical harmonic expansion of $n(\boldsymbol{\theta})$ as

$$a_l^m = \int_{\Omega_S} d\Omega_{\boldsymbol{\theta}} n(\boldsymbol{\theta}) Y_l^{m*}(\boldsymbol{\theta}), \quad (\text{A1})$$

where the integral is over the survey area Ω_S and $*$ denotes a complex conjugate. We shall use the convention of [57] for the spherical harmonics $Y_l^m(\boldsymbol{\theta})$. The dipole vector components in the three dimensional Cartesian coordinates is then defined as $\vec{D} = (-\sqrt{2}\mathcal{R}e(a_1^1), \sqrt{2}\mathcal{I}m(a_1^1), a_1^0)$ where $\mathcal{R}e(f)$ and $\mathcal{I}m(f)$ stand for a real and an imaginary part of some quantity f , respectively (See, e.g., [58]). Accordingly, the magnitude of the dipole is

$$\langle |\vec{D}|^2 \rangle = \sum_{m=-1}^1 \langle |a_1^m|^2 \rangle, \quad (\text{A2})$$

where the angle brackets denote an ensemble average. Given a_l^m , we can estimate the magnitude of the dipole moments of various contributions.

a. *Aberration Induced Dipole*

If the aberration is the only cause of the dipole in the galaxy number density field, the field has the form given by Eq. (8). We define the dipole amplitude due to the aberration effect A_{ab} as

$$\sqrt{|\vec{D}_{\text{ab}}|^2} \equiv \sqrt{\frac{4\pi}{3}} \bar{n}_g A_{\text{ab}}. \quad (\text{A3})$$

where \bar{n}_g is the average angular number density of galaxies per steradian. By evaluating Eqs. (A1) and (A2) using Eq. (8), we can find $A_{\text{ab}} = 2\tilde{\beta}$ for an all-sky survey (and this is the reason for factoring out $\bar{n}_g \sqrt{4\pi/3}$ in the right hand side of the above equation).

b. *Large Scale Structure Dipole*

The coefficient a_l^m from the large scale structure (LSS) may be estimated as

$$\langle |a_{l,\text{LSS}}^m|^2 \rangle = \frac{2}{\pi} \bar{n}_g^2 b_g^2 \int_0^\infty P_m^L(k) |I_l(k)|^2 k^2 dk = \bar{n}_g^2 C_g(l). \quad (\text{A4})$$

We then define the amplitude of the dipole due to large scale structure A_{LSS} as

$$\sqrt{\langle |\vec{D}_{\text{LSS}}|^2 \rangle} = \sqrt{3C_g(1)} \bar{n}_g \equiv \sqrt{\frac{4\pi}{3}} \bar{n}_g A_{\text{LSS}}. \quad (\text{A5})$$

c. *Poisson Shot Noise Dipole*

For the Poisson shot noise, $\langle a_{l,\text{P}}^m \rangle = \bar{n}_g$. We define the amplitude of the dipole due to Poisson noise A_{P} as

$$\sqrt{\langle |\vec{D}_{\text{P}}|^2 \rangle} = \sqrt{3\bar{n}_g} \equiv \sqrt{\frac{4\pi}{3}} \bar{n}_g A_{\text{P}}. \quad (\text{A6})$$

2. Partial-Sky Survey

The incomplete sky coverage may be taken into account by a tensor $W_{ll'}^{mm'}$ [37, 56]. It is defined as

$$W_{ll'}^{mm'} = \oint_{4\pi} d\Omega \boldsymbol{\theta} Y_l^m(\boldsymbol{\theta}) Y_{l'}^{m'*}(\boldsymbol{\theta}) M(\Omega), \quad (\text{A7})$$

where an angular 'mask' $M(\Omega)$ is defined such that $M(\Omega) = 1$ over the area of the sky observed and $M(\Omega) = 0$ elsewhere. This tensor satisfies for any l

$$\frac{1}{2l+1} \sum_{m=-l}^l \sum_{l'=0}^{\infty} \sum_{m'=-l'}^{l'} |W_{ll'}^{mm'}|^2 = \frac{\Omega_S}{4\pi}. \quad (\text{A8})$$

With the tensor $W_{ll'}^{mm'}$, the coefficient of the spherical harmonic expansion for the incomplete sky coverage becomes

$$\langle |c_l^m|^2 \rangle = \sum_{l'=0}^{\infty} \sum_{m'=-l'}^{l'} |W_{ll'}^{mm'}|^2 \langle |a_{l'}^{m'}|^2 \rangle, \quad (\text{A9})$$

where a_l^m is the coefficients for the all-sky survey. We then define the amplitudes of the dipole fluctuation in the galaxy number density field in terms of c_l^m instead of a_l^m . Introducing coefficients $S_{ll'}$ as

$$S_{ll'} = \sum_{m=-l}^l \sum_{m'=-l'}^{l'} |W_{ll'}^{mm'}|^2, \quad (\text{A10})$$

we define the dipole amplitudes from various contributions for a partial-sky survey as

$$A_{LSS} = \sqrt{\frac{3}{4\pi} \sum_{l'=0}^{\infty} S_{1l'} C_g(l')}, \quad (\text{A11})$$

$$A_P = \frac{3}{\sqrt{4\pi}} \sqrt{\frac{\Omega_S}{4\pi\bar{n}_g}}, \quad (\text{A12})$$

and

$$A_{ab} = 2\tilde{\beta} \sqrt{\frac{S_{11'}}{3}}, \quad (\text{A13})$$

which are the equations used to obtain the rough estimates of the signal to noise ratio of the aberration induced dipole in Sec. IV.

Finally, we point out two things. Firstly, for a full-sky survey, $W_{ll'}^{mm'} = \delta_{ll'}^K \delta_{mm'}^K$, and hence $S_{ll'} = (2l+1)\delta_{ll'}^K$. As a result, we recover $A_{ab} = 2\tilde{\beta}$ for such a survey as is expected. Secondly, we note that in a practical computation, we cannot complete the l' summation in Eq. (A11). We have made the summation up to $l' = 500$ for the SDSS DR6 survey geometry and $l' = 200$ for the expected LSST survey geometry considered in this paper. Indeed, it is found that Eq. (A8) satisfies to a good accuracy for these upper limit values for the l' -summation.

$$\frac{1}{3} \sum_{m=-1}^{m=1} \sum_{l'=0}^{l'=500} \sum_{m'=-l'}^{m=l'} |W_{ll'}^{mm'}|^2 = 0.9455 \frac{\Omega_{SDSS}}{4\pi},$$

$$\frac{1}{3} \sum_{m=-1}^{m=1} \sum_{l'=0}^{l'=200} \sum_{m'=-l'}^{m=l'} |W_{ll'}^{mm'}|^2 = 0.9966 \frac{\Omega_{LSST}}{4\pi}.$$

-
- [1] A. Kogut, C. Lineweaver, G. F. Smoot, C. L. Bennett, A. Banday, N. W. Boggess, E. S. Cheng, G. de Amici, D. J. Fixsen, G. Hinshaw, et al., *Astrophys. J.* **419**, 1 (1993).
- [2] C. H. Lineweaver, L. Tenorio, G. F. Smoot, P. Keegstra, A. J. Banday, and P. Lubin, *Astrophys. J.* **470**, 38 (1996).
- [3] S. Courteau and S. van den Bergh, *Astronomical Journal* **118**, 337 (1999).
- [4] W. Dehnen and J. J. Binney, *MNRAS* **298**, 387 (1998).
- [5] M. J. Reid, K. M. Menten, X. W. Zheng, A. Brunthaler, L. Moscadelli, Y. Xu, B. Zhang, M. Sato, M. Honma, T. Hirota, et al., *Astrophys. J.* **700**, 137 (2009).
- [6] D. Lynden-Bell, O. Lahav, and D. Burstein, *MNRAS* **241**, 325 (1989).
- [7] M. A. Strauss, A. Yahil, M. Davis, J. P. Huchra, and K. Fisher, *Astrophys. J.* **397**, 395 (1992).
- [8] S. Zaroubi, ArXiv Astrophysics e-prints (2002), arXiv:astro-ph/0206052.
- [9] P. Erdoğdu and O. Lahav, *Phys. Rev. D.* **80**, 043005 (2009).
- [10] S. Basilakos and M. Plionis, *MNRAS* **373**, 1112 (2006).
- [11] D. D. Kocevski and H. Ebeling, *Astrophys. J.* **645**, 1043 (2006).
- [12] P. Erdoğdu, J. P. Huchra, O. Lahav, M. Colless, R. M. Cutri, E. Falco, T. George, T. Jarrett, D. H. Jones, C. S. Kochanek, et al., *MNRAS* **368**, 1515 (2006).
- [13] R. Watkins, H. A. Feldman, and M. J. Hudson, *MNRAS* **392**, 743 (2009).
- [14] G. Lavaux, R. B. Tully, R. Mohayaee, and S. Colombi, *Astrophys. J.* **709**, 483 (2010).
- [15] G. F. R. Ellis and J. E. Baldwin, *MNRAS* **206**, 377 (1984).
- [16] M. S. Turner, *Phys. Rev. D.* **44**, 3737 (1991).
- [17] R. R. Caldwell, R. Dave, and P. J. Steinhardt, *Physical Review Letters* **80**, 1582 (1998).
- [18] M. Takada, *Phys. Rev. D.* **74**, 043505 (2006).
- [19] C. L. Bennett, A. J. Banday, K. M. Gorski, G. Hinshaw, P. Jackson, P. Keegstra, A. Kogut, G. F. Smoot, D. T. Wilkinson, and E. L. Wright, *Astrophys. J. Lett.* **464**, L1 (1996).
- [20] Y. Jing and L. Fang, *Physical Review Letters* **73**, 1882 (1994).
- [21] G. Efstathiou, *MNRAS* **343**, L95 (2003).
- [22] A. Baleisis, O. Lahav, A. J. Loan, and J. V. Wall, *MNRAS* **297**, 545 (1998).
- [23] C. A. Scharf, K. Jahoda, M. Treyer, O. Lahav, E. Boldt, and T. Piran, *Astrophys. J.* **544**, 49 (2000).
- [24] C. Blake and J. Wall, *Nature* **416**, 150 (2002).
- [25] J. J. Condon, W. D. Cotton, E. W. Greisen, Q. F. Yin, R. A. Perley, G. B. Taylor, and J. J. Broderick, *Astronomical Journal* **115**, 1693 (1998).

- [26] D. G. York, J. Adelman, J. E. Anderson, Jr., S. F. Anderson, J. Annis, N. A. Bahcall, J. A. Bakken, R. Barkhouser, S. Bastian, E. Berman, et al., *Astronomical Journal* **120**, 1579 (2000).
- [27] D. N. Spergel, R. Bean, O. Doré, M. R.olta, C. L. Bennett, J. Dunkley, G. Hinshaw, N. Jarosik, E. Komatsu, L. Page, et al., *Astrophys. J. Suppl.* **170**, 377 (2007).
- [28] M. Fukugita, N. Yasuda, J. Brinkmann, J. E. Gunn, Ž. Ivezić, G. R. Knapp, R. Lupton, and D. P. Schneider, *Astronomical Journal* **127**, 3155 (2004).
- [29] G. Bruzual and S. Charlot, *MNRAS* **344**, 1000 (2003).
- [30] H. F. Stabenau, A. Connolly, and B. Jain, *MNRAS* **387**, 1215 (2008).
- [31] P. J. E. Peebles, *The large-scale structure of the universe* (Princeton, N.J., Princeton University Press, 1980).
- [32] M. Takada and S. Bridle, *New Journal of Physics* **9**, 446 (2007).
- [33] S. Dodelson, *Modern cosmology* (Amsterdam Netherlands, Academic Press, 2003).
- [34] A. J. S. Hamilton, *MNRAS* **312**, 257 (2000).
- [35] M. Tegmark, S. Dodelson, D. J. Eisenstein, V. Narayanan, R. Scoccimarro, R. Scranton, M. A. Strauss, A. Connolly, J. A. Frieman, J. E. Gunn, et al., *Astrophys. J.* **571**, 191 (2002).
- [36] A. Baleisis, O. Lahav, A. J. Loan, and J. V. Wall, *MNRAS* **297**, 545 (1998).
- [37] P. J. E. Peebles, *Astrophys. J.* **185**, 413 (1973).
- [38] J. K. Adelman-McCarthy and the SDSS Collaboration, ArXiv e-prints (2007), 0707.3413.
- [39] M. Fukugita, T. Ichikawa, J. E. Gunn, M. Doi, K. Shimasaku, and D. P. Schneider, *Astronomical Journal* **111**, 1748 (1996).
- [40] J. E. Gunn, M. Carr, C. Rockosi, M. Sekiguchi, K. Berry, B. Elms, E. de Haas, Ž. Ivezić, G. Knapp, R. Lupton, et al., *Astronomical Journal* **116**, 3040 (1998).
- [41] K. Yahata, A. Yonehara, Y. Suto, E. L. Turner, T. Broadhurst, and D. P. Finkbeiner, *Publications of the Astronomical Society of Japan* **59**, 205 (2007).
- [42] D. J. Schlegel, D. P. Finkbeiner, and M. Davis, *Astrophys. J.* **500**, 525 (1998).
- [43] J. R. I. Gott, M. Jurić, D. Schlegel, F. Hoyle, M. Vogeley, M. Tegmark, N. Bahcall, and J. Brinkmann, *Astrophys. J.* **624**, 463 (2005).
- [44] D. J. Eisenstein and W. Hu, *Astrophys. J.* **511**, 5 (1999).
- [45] C. W. Stubbs, D. Sweeney, J. A. Tyson, and LSST, in *Bulletin of the American Astronomical Society* (New York, American Institute of Physics, 2004), vol. 36, p. 1527.
- [46] Z. Ivezić, A. J. Tyson, M. A. Strauss, S. Kahn, C. Stubbs, P. Pinto, K. Cook, and LSST Collaboration, in *Bulletin of the American Astronomical Society* (New York, American Institute of Physics, 2006), vol. 38, p. 1017.
- [47] D. Huterer, M. Takada, G. Bernstein, and B. Jain, *MNRAS* **366**, 101 (2006).
- [48] F. Crawford, *Astrophys. J.* **692**, 887 (2009).
- [49] N. Kaiser, H. Aussel, B. E. Burke, H. Boesgaard, K. Chambers, M. R. Chun, J. N. Heasley, K. Hodapp, B. Hunt, R. Jedicke, et al., in *Society of Photo-Optical Instrumentation Engineers (SPIE) Conference Series*, edited by J. A. Tyson & S. Wolff (Bellingham, WA, SPIE, 2002), vol. 4836, p. 154.
- [50] A. Kashlinsky, F. Atrio-Barandela, D. Kocevski, and H. Ebeling, *Astrophys. J. Lett.* **686**, L49 (2008).
- [51] J. Chluba, G. Hütsi, and R. A. Sunyaev, *A&A* **434**, 811 (2005).
- [52] S. Ho, S. Dedeo, and D. Spergel, ArXiv e-prints (2009), 0903.2845.
- [53] A. Kashlinsky, F. Atrio-Barandela, D. Kocevski, and H. Ebeling, *Astrophys. J.* **691**, 1479 (2009).
- [54] A. Kashlinsky, F. Atrio-Barandela, H. Ebeling, A. Edge, and D. Kocevski, *Astrophys. J.* **712**, L81 (2010).
- [55] J. P. Ostriker and E. T. Vishniac, *Astrophys. J. Lett.* **306**, L51 (1986).
- [56] C. Scharf, Y. Hoffman, O. Lahav, and D. Lynden-Bell, *MNRAS* **256**, 229 (1992).
- [57] J. D. Jackson, *Classical electrodynamics; 3rd ed.* (Wiley, New York, NY, 1999).
- [58] C. J. Copi, D. Huterer, and G. D. Starkman, *Phys. Rev. D* **70**, 043515 (2004).
- [59] In General Relativity terms, the comoving hypersurface, where the energy flux of matter comoving with the cosmic expansion vanishes, has stayed the same from the last scattering surface to the present-day Universe.
- [60] In fact, we will consider flux limited as well as redshift limited samples in this paper (see Table II). Because redshifts of galaxies ahead of our motion have systematically smaller than those behind us, there arises an additional dipolar variation in the number density. Up to $O(\beta)$ and assuming we study galaxies in the redshift range $z_1 \leq z \leq z_2$, we can take account of this effect by writing

$$\tilde{\beta} = (1 + 1.25x(1 - p) + F(z_1, z_2))\beta.$$

instead of Eq. (9) where

$$2F(z_1, z_2) = \left[(1 + z_1)n_g(z_1) - (1 + z_2)n_g(z_2) + \int_{z_1}^{z_2} n_g(z)dz \right],$$

where $n_g(z)$ is the galaxy redshift distribution in the matter rest frame. Assuming Eq. (29) for $n_g(z)$ with $z_0 = 0.1$ for SDSS or $z_0 = 0.4$ for LSST, one can show that $F(0.1, 0.4) = 0.33$ (SDSS shallow sample), $F(0.1, 0.9) = 1.4$ (SDSS deep sample), or $F(1, \infty) = 0.91$ (LSST). Hence $F(z_1, z_2)$ is positive and $O(1)$ in the case studies in this paper.

- [61] Here we simply ignore the square pixel shape and also the masking effect within one pixel. However, our approximation is good enough for the large-angle cross-correlations.